

NONCOHERENT COMMUNICATION THEORY FOR COOPERATIVE
DIVERSITY IN WIRELESS NETWORKS

A Thesis

Submitted to the Graduate School
of the University of Notre Dame
in Partial Fulfillment of the Requirements
for the Degree of

Master of Science
in Electrical Engineering

by

Deqiang Chen, B.S.

J. Nicholas Laneman, Director

Graduate Program in Electrical Engineering

Notre Dame, Indiana

May 2004

NONCOHERENT COMMUNICATION THEORY FOR COOPERATIVE DIVERSITY IN WIRELESS NETWORKS

Abstract

by

Deqiang Chen

In a wireless network, users can relay information to exploit cooperative diversity, thereby increasing reliability and reducing power consumption. This thesis focuses on noncoherent communication theory for cooperative diversity.

This thesis develops a general framework for maximum likelihood (ML) demodulation for cooperative diversity with a decode-and-forward protocol at the relays. A piecewise-linear (PL) demodulator is developed as an accurate approximation of nonlinear ML detectors. This PL detector leads to an involved yet closed-form approximation for the error probability of ML detectors. Numerical results show that the approximation is very tight. Analysis based on the Bhattacharyya upper bound suggests cooperative diversity with decoding relays does not achieve full diversity order. This conclusion is supported by the high SNR approximation of error probability obtained from the PL approximation. This thesis also presents some results about the application of convolutional codes in cooperative diversity. Given the same spectral efficiency, simulation results suggest that cooperative diversity can perform better than non-cooperative single-hop in the block fading channel given both schemes use ML detectors designed for the i.i.d. fading channel.

In memory of Grandma

CONTENTS

FIGURES	v
ACKNOWLEDGMENTS	vii
CHAPTER 1: INTRODUCTION	1
CHAPTER 2: BACKGROUND	6
2.1 Information-Theoretic Perspective	6
2.2 Communication-Theoretic Perspective	7
2.3 Motivation	8
CHAPTER 3: UNCODED NONCOHERENT MODULATION AND DEMOD- ULATION IN COOPERATIVE DIVERSITY	10
3.1 System Model	11
3.1.1 Notation	11
3.1.2 Model	11
3.2 Noncoherent Decode-and-Forward	13
3.2.1 Maximum Likelihood Detector	13
3.2.2 Piecewise-Linear Detector and Performance	15
3.2.3 High SNR Approximation	18
3.2.4 Analysis of Diversity Order for Cooperative Diversity with Multiple Relays	19
3.3 Numerical Results	21
3.4 Issues of Amplify-and-Forward in Noncoherent Cooperative Diversity	25
CHAPTER 4: EXTENSION OF PIECEWISE-LINEAR TECHNIQUES	31
4.1 Coherent Cooperative Diversity with the Piecewise-Linear Detector	32
4.2 Noncoherent Cooperative Diversity with Two Decoding Relays	33
4.3 Noncoherent Cooperative Diversity With Two Receive Antennas	43

CHAPTER 5: APPLICATION OF CONVOLUTIONAL CODES IN COOP- ERATIVE DIVERSITY	54
5.1 Introduction	54
5.1.1 Summary of Assumptions and Results	55
5.2 System Model	57
5.2.1 Notation	57
5.2.2 Model	57
5.3 Maximum Likelihood Sequence Detection for Noncoherent Coopera- tive Diversity	58
5.3.1 Detector For I.I.D. Fading Channel	58
5.3.2 Analysis of Performance	60
5.3.3 Issues in Noncoherent ML Detection for Block Fading Channel	65
5.4 Numerical Results	67
 CHAPTER 6: CONCLUDING REMARKS AND FUTURE WORK	 71
 BIBLIOGRAPHY	 73

FIGURES

1.1	Example for cooperative diversity.	2
3.1	Block diagram for cooperative diversity with multiple relays.	12
3.2	General detector structure for cooperative diversity with multiple relays.	14
3.3	Plot of the function $f_i(t_i)$ with different average error probabilities for the relay.	15
3.4	Error probability performance of cooperative diversity with a decoding relay located at (0.1,0), <i>i.e.</i> , close to the source.	22
3.5	Error probability performance of cooperative diversity with a decoding relay located at (0.5,0), <i>i.e.</i> , halfway between the source and destination.	23
3.6	Error probability performance of cooperative diversity with a decoding relay located at (0.9,0), <i>i.e.</i> , close to the destination.	24
3.7	Compare the results from PL approximation and high SNR approximation with simulation results for noncoherent cooperative diversity with a decoding relay located at (0.1,0), <i>i.e.</i> , close to the source.	26
3.8	Compare the results from PL approximation and high SNR approximation with simulation results for noncoherent cooperative diversity with a decoding relay located at (0.5,0), <i>i.e.</i> , halfway between the source and destination.	27
3.9	Compare the results from PL approximation and high SNR approximation with simulation results for noncoherent cooperative diversity with a decoding relay located at (0.9,0), <i>i.e.</i> , close to the destination.	28
4.1	Error probability of coherent BFSK with the decoding relay located at (0.1,0), <i>i.e.</i> , close to the source.	34
4.2	Error probability performance of coherent BFSK with the decoding relay located at (0.5,0), <i>i.e.</i> , in the middle of source and destination.	35
4.3	Error probability performance of coherent BFSK with the decoding relay located at (0.9,0), <i>i.e.</i> , close to the destination.	36

4.4	Error probability of noncohernt BFSK with two decoding relays. The relays are located at $(0.1,0)$, <i>i.e.</i> , close to the source.	44
4.5	Error probability of noncohernt BFSK with two decoding relays. The relays are located at $(0.5,0)$, <i>i.e.</i> , halfway between the source and destination.	45
4.6	Error probability of noncohernt BFSK with two decoding relays. The relays are located at $(0.9,0)$, <i>i.e.</i> , close to the destination.	46
4.7	Detector for cooperative diversity with two receive antennas.	47
4.8	Comparison between single-hop with three receive antennas and cooperative diversity with two receive antennas at the destination. The relay is located at $(0.1,0)$, <i>i.e.</i> , close to the source.	51
4.9	Comparison between single-hop with three receive antennas and cooperative diversity with two receive antennas at the destination. The relay is located at $(0.5,0)$, <i>i.e.</i> , halfway between the source and destination.	52
4.10	Comparison between single-hop system with three receive antennas and cooperative diversity with two receive antennas at the destination. The relay is located at $(0.9,0)$, <i>i.e.</i> , close to the destination. . .	53
5.1	Diagram of channel uses by single-hop and cooperative diversity. Each block indicates a symbol transmitted in channel.	57
5.2	Average bit error probability of noncoherent BFSK with the decoding relay located at different locations. Soft decoding based on the Viterbi algorithm is used. The fading coefficients are assumed to be i.i.d. between symbols.	68
5.3	Average bit error probability of noncoherent BFSK with the decoding relay located at different locations. Soft decoding based on the Viterbi algorithm is used. The length of the fading block is assumed to cover eight symbol-periods.	69
5.4	Average bit error probability of noncoherent BFSK with the decoding relay located at different locations. Soft decoding based on the Viterbi algorithm is used. The length of the fading block is assumed to cover 128 symbol-periods.	70

ACKNOWLEDGMENTS

A lot of credit for this thesis should go to my advisor, Dr. J. Nicholas Lane-man. I have benefited tremendously from countless interactions and discussions with him. His insight on the fundamental nature of techniques and problems has not only inspired me but also helped me better understand the meaning of research. I would also like to thank the other members of my thesis committee for many useful interactions and for contributing their broad perspectives to this thesis.

I have gained help and support from a lot of other people since I came to Notre Dame. I cannot fully express my appreciation with a few words here. Thanks go to Wenyi Zhang, Xun Liu and Shivaprasad Kotagiri for many technical discussions. Thanks also go to Hui Fang, Shaoping Shen, for kindly helping me get used to life here and playing soccer regularly.

In addition, I would like to present this thesis in honor of my grandmother, who passed away last year. Her love has been one of the biggest debts that I can never pay back. I also thank my parents for supporting and encouraging me through these many years. As their only son, I regret that I cannot be with them for most of the time and thank them for their understanding and support. I also thank Li Xie. Her understanding and encouragement has meant more than what I can express in a few words here.

CHAPTER 1

INTRODUCTION

Relying on the propagation of electromagnetic waves in free space, wireless communications has given people the freedom to communicate from almost anywhere, even when they are traveling. However, the wireless channel in free space has proven to be quite hostile as the signals suffer significant attenuation, shadowing, noise, interference, *etc.* [21]. Among the countless efforts to guarantee the quality of service under this hostile environment, this thesis focuses on how to combat path loss and fading.

Path loss, or large-scale path loss, significantly reduces the strength of transmitted signals such that the signal-to-noise-ratio (SNR) at the receiver can be very low. There are a number of different models for path loss [21]. Most of them suggest an inverse relationship between the path loss and the transmitted distance. To combat the path loss, the transmitter power can be increased. However, the power can not be increased without limit. Another method is to place some repeaters between the transmitter and receiver to periodically amplify the signals or detect and regenerate the signals. The latter method proves to be more efficient than increasing of the power, even when total power is normalized.

Fading, also called the small-scale path loss, comes from the multipath propagation of signals. Fading significantly degrades the performance of wireless communication systems. For example, the probability of error for binary-phase-shift-keying

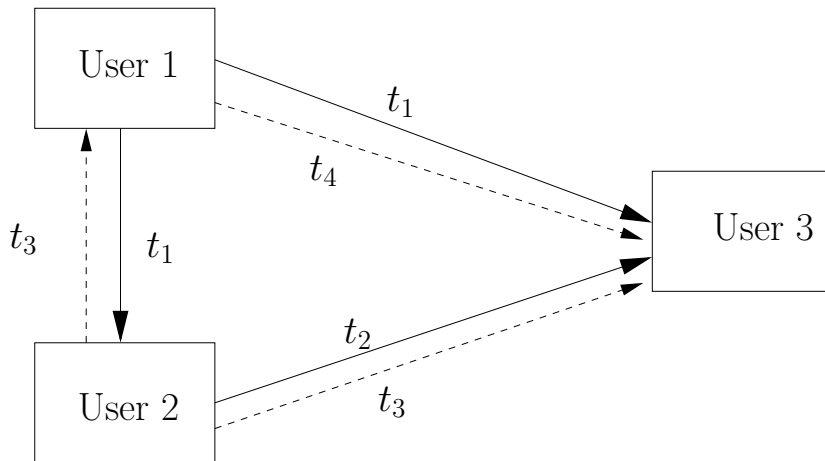


Figure 1.1. Example for cooperative diversity.

(BPSK) in the additive white Gaussian noise (AWGN) channel decreases exponentially in SNR [20]. However, if Rayleigh fading is considered, the probability of error only decreases as $1/\text{SNR}$ [20]. Diversity techniques have been widely accepted as one of the effective ways to combat multipath fading in wireless communications [20]. Among other approaches, multiple transmit or receive antennas at the same terminal are often desirable for spatial diversity. However, in many scenarios, such as in cellular, ad hoc or sensor networks, multiple antennas can often be precluded due to the size limitations of terminals.

Cooperative diversity [23, 24, 14] combines the idea of intermediate repeaters and multiple antennas. It avoids the size limitations of multiple antennas at the same terminal and provides spatial diversity by allowing the terminals to relay in parallel, thus sharing multiple antennas belonging to different terminals.

The basic idea of user cooperative diversity can be seen in Fig. 1.1. It shows a scenario in which both users, namely user 1 and user 2, want to communicate with a third user, *i.e.*, user 3. This can be a common scenario for ad hoc networks. It can also occur in a mobile network in which user 3 can be the base station.

Cooperative diversity means that these two users form a group to help each other transmit the information more reliably. A simple way for them to do this can be as follows. Assuming a time-division-multiple-access (TDMA) system, user 1 sends the information to user 3 at time t_1 . Due to the nature of the wireless transmission, user 2 can receive the communication from the source to destination at time t_1 . At time t_2 , after some processing, the relay can send signals to the destination. These signals include information that the source wants to transmit to the destination at time t_1 . In the following time slots t_3 and t_4 , user 1 and user 2 switch roles, with user 2 sending its own information and user 1 acting as a relay. In most wireless networks, the two channels, namely, the channel between user 1 and user 3 and the channel between user 2 and user 3, suffer independent fading as they are located in different places. As the signals for the same information received by the destination pass through two independent channels, spatial diversity can be achieved by diversity combining techniques, and better performance can be obtained. This thesis focuses mostly on the transmission of information between user 1 and user 3 with user 2 serving as a relay. Although this example is based on TDMA, cooperative diversity is not limited to this particular accessing method. For example, cooperative diversity based on code-division-multiple-access (CDMA) has been proposed in [23, 24].

The outline of the following chapters is as follows. Chapter 2 presents a literature survey for cooperative diversity from different perspectives. It highlights the subtlety and flexibility of the cooperative diversity channel. It also provides the motivation for exploring noncoherent cooperative diversity. Chapter 3 considers noncoherent modulation and demodulation for cooperative diversity and develops a general framework for maximum likelihood (ML) demodulation in cooperative diversity with a decode-and-forward protocol at the relays. It develops a piecewise-linear demodulator as an accurate approximation of the nonlinear ML detector.

This piecewise-linear detector not only leads to a tight, closed-form approximation for the error probability of the ML detector, but also has certain implementation advantages. Based on this closed-form result, this thesis derives a high SNR approximation for the noncoherent decode-and-forward system, which suggests that an optimal location for the relay can be different from that of the coherent amplify-and-forward system. Chapter 4 extends the piecewise-linear detector in Chapter 3 to the cases of coherent cooperative diversity with a decoding relay, cooperative diversity with two parallel relays and cooperative diversity with multiple antennas. It illustrates the details of how to employ the piecewise-linear approximation to obtain a tight closed-form approximation for the probability of error. Chapter 5 explores the problem of combining coding with noncoherent cooperative diversity and provides some preliminary results. Focusing on convolutional codes, this chapter develops noncoherent ML detectors for the independent identically distributed (i.i.d.) fading channel. It shows the main advantage of cooperative diversity relies on spatial diversity. Given the spectral efficiency constraint, future work for cooperative diversity should be more focused on the block fading channel.

The main contribution of this thesis can be summarized as following:

- A general framework is proposed for ML demodulation of both coherent and noncoherent cooperative diversity with decoding relays.
- A piecewise-linear (PL) detector is developed to closely approximate the non-linear ML detector for the decode-and-forward protocol. This PL detector is also extended to coherent cooperative diversity with a decoding relay.
- Based on the PL detector, a closed-form expression is presented for the uncoded bit error rate (BER) of noncoherent cooperative diversity with a decoding relay. The uncoded BER based on the PL detector for coherent cooperative diversity with a decoding relay is expressed as an integration. The PL detector is also extended to cooperative diversity with two relays and cooperative diversity with two antennas and yields closed-form expressions for noncoherent uncoded BER. Numerical results show that all these expressions provide tight approximations of the performance of ML detectors. Thus, the PL detector is applicable to both coherent and noncoherent cooperative diversity with decoding relays. It not only leads to tight approximations for the error probability of ML detectors, but also has certain implementation advantages.

- Based on the involved closed-form expression from PL approximation, a high SNR approximation of the BER is provided for noncoherent cooperative diversity with a decoding relay. It is more concise, but provides a tight approximation in high SNR regimes. It also suggests that the optimal location for a decoding relay can be different from that of an amplifying relay [22], although numerical results indicate that these two optimum locations are quite close. The high SNR approximation also suggests that cooperative diversity with a decoding relay does not achieve full diversity order 2.
- It is shown that the diversity order d for cooperative diversity with $M - 1$ decoding relays is bounded by $1 + (M - 1)/2 \leq d \leq M$.
- We show that it is possible to use the amplify-and-forward protocol at the relay even without CSI. However, we also point out the ML detection here poses a particular challenge. The ML detector involves the ratio of two integrals that must be evaluated numerically.
- Noncoherent and coherent ML sequence detectors are presented for cooperative diversity with convolutional codes in the i.i.d. fading channel. These detectors can be easily implemented via the Viterbi algorithm. Our analysis provides a common expression of the Bhattacharyya upper bounds for cooperative diversity in the i.i.d. fading channel with different signaling, namely noncoherent BFSK, coherent BFSK and BPSK. The expression shows that the free distance of the convolutional code is a key factor for coding performance in cooperative diversity for the i.i.d. fading channel. This common expression also indicates that there is about a 3 dB loss for noncoherent BFSK compared to coherent BFSK for cooperative diversity in the i.i.d. fading channel.
- The diversity order for noncoherent cooperative diversity with convolutional codes is less than $2d_{\text{free}}$ in the i.i.d. fading channel. The loss of diversity gain in cooperative diversity may come from the choice of a decode-and-forward protocol at the relay. Given that single-hop and cooperative diversity use maximum free distance convolutional codes with the same constraint length, the analysis indicates that cooperative diversity does not perform better than single-hop in the noncoherent i.i.d. fading channel given the same spectral efficiency.
- Using ML detectors designed for the i.i.d. fading channel, simulation results suggest that cooperative diversity can perform better than single-hop in the block fading channel given the same spectral efficiency. Optimization of the location of the relay is still critical in obtaining the improvement of performance.

CHAPTER 2

BACKGROUND

This chapter provides a survey of the existing literature about cooperative diversity. The current results of cooperative diversity are classified into two categories, namely information-theoretic and communication-theoretic perspectives. The information-theoretic results are concerned with the capacity of cooperative diversity, and the communication-theoretic results are more concerned with the performance of cooperative diversity with some particular modulation or coding schemes.

2.1 Information-Theoretic Perspective

Cooperative diversity can be viewed as a special case of the multiple-access channel with “generalized” feedback between the transmitting terminals [32, 33]. The difference is that the “generalized” feedback output to the encoder might be related with the output of the decoder at the destination; but in cooperative diversity, the feedback is simply the signals observed by the relay. The following results are all focused on cooperative diversity.

Assuming the channel state information (CSI) is available to the transmitters, it is demonstrated in [23, 24] that cooperative diversity increases the sum-rate over the non-cooperative transmission for ergodic fading. It also shows that cooperative diversity improves the outage performance for non-ergodic fading and decreases the sensitivity of the achievable data rate to the variations of the channels.

For the case that CSI is unavailable to the transmitters but available to the receivers, it is shown in [12] that cooperative diversity does not increase the maximum

sum-rate comparing with the non-cooperative transmission. A variety of algorithms that can achieve full diversity order for cooperative diversity are proposed in [12].

Cooperative diversity decreases bandwidth efficiency with the number of cooperating terminals since the orthogonal channel assumption in cooperative diversity requires the relay not to transmit and receive at the same time. The practical side of this assumption lies in the fact that the transmitting powers are much higher than the receiving signal powers if they are in the same frequency band. Algorithms based upon space-time codes are proposed in [15] to improve the bandwidth efficiency by allowing all relays to transmit on the same subchannel. Requiring more computational complexity in the terminals, these space-time coded cooperative diversity algorithms also achieve spatial diversity benefits. The design of distributed space-time filtering (STF) schemes is also proposed in [4]. It also develops a necessary and sufficient condition for ensuring the full diversity advantage. An interesting conclusion is that the an optimal design for the distributed implementation may not be optimal in the point-to-point scenario.

2.2 Communication-Theoretic Perspective

In [14], maximum likelihood (ML) detectors and the corresponding analysis, in terms of uncoded bit error rate, are developed for coherent cooperative diversity. It is also pointed out that systems with an amplifying relay appear to perform comparably, if not better, than systems with a decoding relay. Due to the relative simplicity of the amplify-and-forward protocol, this has inspired several extensions [5, 22]. Using a moment-generating function method, [5] proposes a “blind” relay that does not require instantaneous CSI between the source and relay, but it can not satisfy the instantaneous power constraint. Building upon methods from [30], [22] provides closed-form approximations of the average symbol error probability (SEP) for general multi-branch, multi-hop cooperative diversity for asymptotically high SNR. It also demonstrates that, in the sense of minimizing SEP with sufficiently high SNR, it is best for a single amplifying relay to be in a location that has the same distance from the source and destination.

The problem of combining channel codes with cooperative diversity has been considered in [8, 9, 35, 17]. A key feature in [8] is that the information sequences

are not simply repeated by the partner on a symbol-by-symbol basis. Instead, [8] suggests partitioning the codeword of each user into two subblocks; one subblock is transmitted by the user and the other by the partner whenever possible. This is referred to as “coded cooperation”. It is shown that cooperative diversity with coding achieves impressive gains compared to a non-cooperative system given the same information rate, transmit power, and bandwidth.

In particular, the existence of the relay provides an opportunity for the code word to be interleaved and thus provide a distributed turbo coded system. This idea is demonstrated in [35, 17, 9]. In [35], recursive systematic convolutional (RSC) codes are generated in the source and transmitted to the relay and destination. The relay decodes, interleaves, and then encodes the sequence with the same RSC code. The destination can use a standard turbo decoder. In [17], the source generates a turbo coded sequence and then punctures it before it is sent. The relay decodes and generates the punctured part of the source sequence and sends it to the destination. In [9], similar ideas about turbo codes in cooperative diversity are explored based on coded cooperation [8].

In [34], the diversity order effects of various processing schemes at the destination are investigated for cooperative diversity with up to two amplifying relays. The results show that the diversity order is equal to the number of independent links combined at the destination. Thus, a network with M relays can provide up to $M+1$ order diversity gain. On the other hand, the combination of correlated links does not provide diversity but extra coding gains due to repetition of information.

The case in which the users can have more than one antenna has been considered in [27, 26] to show that cooperative diversity can be exploited together with spatial diversity from multiple transmit or receive antennas. However, it is not clear that whether the combination of cooperative diversity with multiple antennas will continue to substantially improve the performance if the number of relays or antennas is large.

2.3 Motivation

All of the previous work discussed above assumes that each receiver accurately estimates the fading coefficients along the corresponding path. If fading varies slowly,

such CSI might be obtained via estimating training sequences in the protocol headers [21]. However, CSI cannot not be accurately obtainable if the fading coefficients vary quickly within the period of one transmission block. As the coherence time decreases, the estimation of CSI reduces the effective transmission rate substantially since pilot tones must be inserted frequently. In these scenarios, noncoherent modulation and demodulation can be more practical. In addition, noncoherent modulation and demodulation are robust methods for realizing control signaling in wireless networks. To the best of our knowledge, there has not been a comprehensive treatment of noncoherent demodulation for cooperative diversity. This has been the motivation for our work.

CHAPTER 3

UNCODED NONCOHERENT MODULATION AND DEMODULATION IN COOPERATIVE DIVERSITY

As we discussed in Chapter 2, modulation and demodulation for coherent cooperative diversity have been extensively investigated by [14, 5, 22], but little is known for noncoherent cooperative diversity. In this chapter, we focus on modulation and demodulation for noncoherent cooperative diversity.

In the following sections, we develop:

1. A general framework for ML demodulation of both coherent and noncoherent cooperative diversity with decoding relays.
2. A piecewise-linear (PL) detector is developed to closely approximate the non-linear ML detector for noncoherent cooperative diversity with decoding relays. This PL detector is also extended to coherent cooperative diversity with a decoding relay.
3. Based on the PL detector, a closed-form expression for the uncoded bit error rate (BER) of noncoherent cooperative diversity with a decoding relay is presented. Numerical results show that this expression provide a tight approximations of the performance of ML detectors. The PL detector not only leads to a tight approximation for the error probability of ML detectors, but also has certain implementation advantages.
4. Based on the involved closed-form expression from PL approximation, a high SNR approximation is provided for noncoherent cooperative diversity with a decoding relay. It is more concise, but provides a tight approximation in high SNR regimes. It also suggests that the optimal location for a decoding relay can be different from that of an amplifying relay [22] although numerical results indicate that these two optimum locations are quite close. The high SNR approximation also suggests that cooperative diversity with a decoding relay does not achieve full diversity order 2.
5. It is shown that the diversity order d for cooperative diversity with $M - 1$ decoding relays is bounded by $1 + (M - 1)/2 \leq d \leq M$.

The remainder of this chapter is organized as follows. Section 3.1 describes the channel model used in the chapter. Section 3.2 develops a general framework for ML detection for both coherent and noncoherent cooperative diversity. For decode-and-forward cooperative diversity, ML detectors are generally nonlinear functions, which substantially complicates their analysis. As a practical alternative, for purposes of both implementation and analysis, we develop a piecewise-linear detector that closely approximates the ML detector and provides a tight upper bound on its performance. A high SNR approximation is also presented. For the completeness of this thesis, Section 3.4 describes issues for ML detection in noncoherent amplify-and-forward and points out the complexity of this problem. At the end, Section 3.3 presents the simulation results and draws conclusions.

3.1 System Model

3.1.1 Notation

We adopt the following the notation. Vectors and sequences are denoted in bold (*e.g.*, \mathbf{x}) with the i th element denoted as x_i . Random variables are denoted using the sans serif font (*e.g.*, x) while random vectors and sequences are denoted with bold sans serif (*e.g.*, \mathbf{x}). The vector is assumed in column form unless otherwise stated. Calligraphic letters denote events (*e.g.*, \mathcal{R}). The probability density function (pdf) of the random variable x is usually written as $p(x)$.

3.1.2 Model

As shown in Fig. 3.1, the *source* terminal broadcasts the signal x_0 to the *relays* and *destination* in the first subchannel. The relays, denoted as R_i , $i = 1, \dots, M - 1$, and destination receive y_0 and y_i , respectively. After some processing, the relays retransmit signals to the destination in the remaining $M - 1$ orthogonal subchannels.

For the signal processing schemes for the relay, amplify-and-forward and decode-and-forward have been suggested in [14] for coherent demodulation. To model the effect that circuits for transmitters can only work linearly in some power regime, the energy of a symbol transmitted by a relay is constrained to E_i . We refer to this as an instantaneous power constraint in the following. It is shown in Section 3.4 that the detection and analysis for amplify-and-forward becomes mathematical intractable

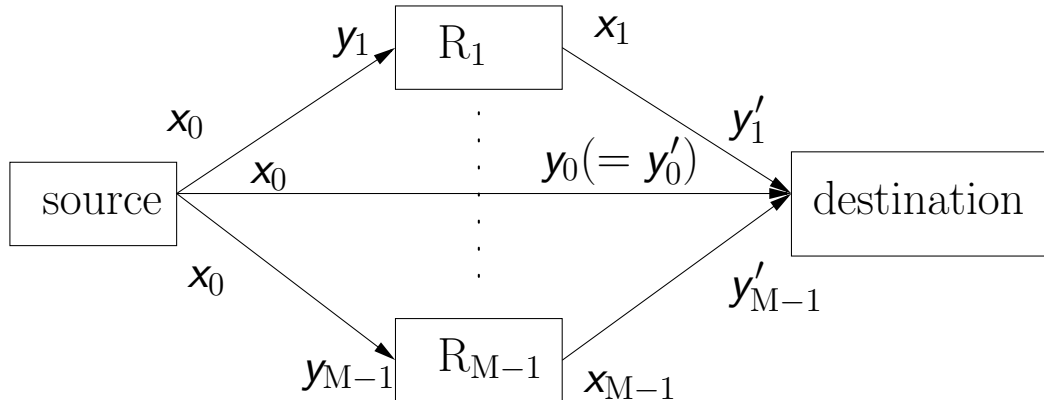


Figure 3.1. Block diagram for cooperative diversity with multiple relays.

in order to satisfy the instantaneous power constraint. For the decode-and-forward protocol, the relays demodulate and retransmit the source signal and thereby avoid power saturation. In addition, the decode-and-forward protocol provides more flexibility for a variety of post-processing methods at the relay if channel coding is employed [8, 9, 27, 26]. Thus, to ensure a power constraint at the relay with potential coding applications in mind, we focus on the decode-and-forward protocol in the remainder of this thesis.

Overall, the destination receives signals y_0, y'_i from M orthogonal channels. To make the notation more compact, we also define $y'_0 = y_0$. After passing these signals through the appropriate matched filters, we obtain a baseband-equivalent discrete-time model. We focus throughout the chapter on binary frequency-shift keying (BFSK) for simplicity of exposition. Assume that the bandwidth of cooperative diversity is larger than the coherence bandwidth of the channel, for BFSK signaling, the outputs from the matched filters can be modeled as

$$\begin{aligned}
 y'_{i1} &= (1 - x_i) \sqrt{E_i} a_{i,M} + n'_{i1}, \\
 y'_{i2} &= x_i \sqrt{E_i} a_{i,M} + n'_{i2},
 \end{aligned} \tag{3.1}$$

where x_i is the symbol sequence transmitted by transceiver i taking values $\{0, 1\}$, E_i is the average symbol energy of the source and relays, $a_{i,j}$ represents the fading coefficient of the corresponding path between transceiver i and j , and n_{i1} and n_{i2} are additive white Gaussian noise (AWGN). For y'_{i1}, y'_{i2} , the subscript i denotes that this

signal is corresponding to symbol x_i and the second subscript, *i.e.*, 1 and 2, denotes the first and second complex baseband signal corresponding to BFSK modulation.

The fading coefficients $\mathbf{a}_{i,j}$ are modeled as zero mean, circularly symmetric mutually independent complex Gaussian random variables with variances $\sigma_{\mathbf{a}_{i,j}}^2$, and the additive noises \mathbf{n}_{ij} are modeled as zero mean, white complex Gaussian random variables with variance N_0 . The average signal noise ratio is defined as

$$\bar{\gamma}_{i,j} \triangleq \sigma_{\mathbf{a}_{i,j}}^2 \mathbf{E}_i / N_0. \quad (3.2)$$

3.2 Noncoherent Decode-and-Forward

In this section, ML detectors are developed for noncoherent cooperative diversity with a decoding relay. Since ML detectors are nonlinear functions, a piecewise-linear approximation is proposed. The piecewise-linear approximation not only leads to a closed-form expression for uncoded BER, but also has some implementation advantages.

3.2.1 Maximum Likelihood Detector

The ML detector will be implemented as shown in Fig 3.2. This detector structure extends immediately to all coherent and noncoherent binary modulation formats by properly defining functions $g_i(y'_{i1}, y'_{i2})$ and $f_i(t_i)$. Thus, it provides a unified framework for the analysis. It might facilitate changes between different transmission formats according to system requirements.

Using the fact that the noise in the orthogonal channels is independent, the destination observations are conditionally independent given the transmitted signal and average error probability of the relay. The ML detector for the noncoherent cooperative diversity system can be shown to employ the functions

$$g_i(y'_{i1}, y'_{i2}) = \frac{\mathbf{E}_i \sigma_{\mathbf{a}_{i,M}}^2}{(\mathbf{E}_i \sigma_{\mathbf{a}_{i,M}}^2 + N_0) N_0} (|y'_{i1}|^2 - |y'_{i2}|^2), \quad (3.3)$$

and

$$f_i(t_i) = \ln \frac{(1 - \epsilon_i) e^{t_i} + \epsilon_i}{\epsilon e^{t_i} + (1 - \epsilon_i)}, \quad (3.4)$$

where ϵ_i is the average probability of error at the relay R_i , which uses a conventional envelope detector. Note that $t_i \triangleq g_i(y'_{i1}, y'_{i2})$. Fig. 3.3 shows the plot of the function

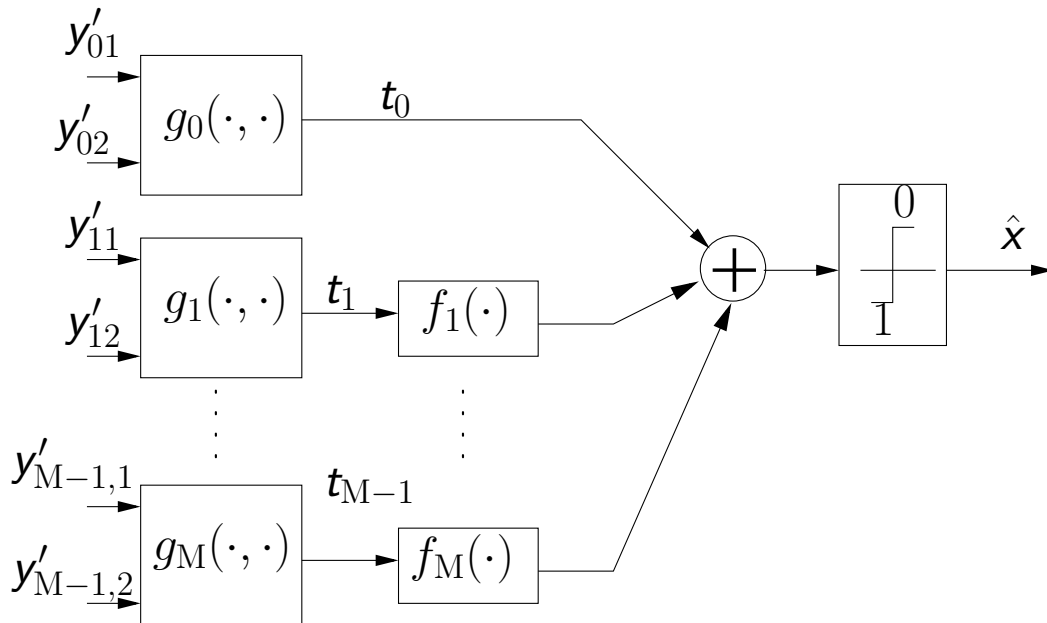


Figure 3.2. General detector structure for cooperative diversity with multiple relays.

(3.4) with different average error probabilities for the relay. It clearly demonstrate the nonlinear behavior of (3.4)¹. The analysis of the diversity transmission must consider the nonlinear behavior of (3.4), which significantly complicates the effort of obtaining a closed-form solution for the probability of error at the destination.

An interpretation of this detector structure from detection and estimation theory is as follows. The matched filter outputs are processed by a function $g_i(r_1, r_2)$ to produce sufficient statistics. Taking a sufficient statistic as input, the function $f_i(t)$ essentially clips its input using the statistical knowledge of the transmission link. Although this ML detector can be applied to the case of multiple parallel relays and multiple antennas at the destination, the remainder of this chapter focuses in the sequel on the case of one relay to illustrate the idea of this piecewise-linear approximation. Chapter 4 demonstrates the flexibility of this ML detector structure by considering two examples, namely cooperative diversity with two parallel relays and cooperative diversity with two antennas at the destination.

¹Note that the behavior of this function resembles that of the classical sigmoid function in neural network.

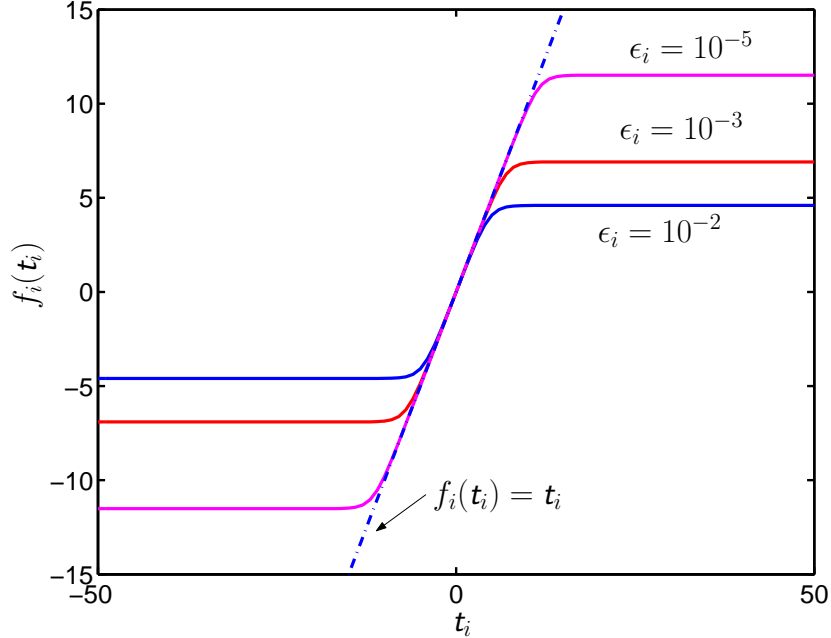


Figure 3.3. Plot of the function $f_i(t_i)$ with different average error probabilities for the relay.

3.2.2 Piecewise-Linear Detector and Performance

As noted in [14], $f_i(t_i)$ essentially “clips” to the values of $\pm \ln[\epsilon_i/(1 - \epsilon_i)]$ for large inputs, and is approximately linear between these extreme values for small inputs. Thus in the sequel we develop a piecewise-linear approximation to $f_i(t_i)$. This approximation suggests an alternative detector, which we call the piecewise-linear (PL) detector, that might be more amenable to practical implementation. Furthermore, as we will see, this detector’s performance provides a tight upper bound on the error probability of the ML detector.

Assuming $\epsilon_1 < 1/2$, our PL detector is obtained from the approximation

$$f_1(t) \cong f_{PL}(t) = \begin{cases} -T_a & \text{for } t < -T_a \\ t & \text{for } -T_a \leq t \leq T_a \\ T_a & \text{for } t > T_a \end{cases}, \quad (3.5)$$

where $T_a \triangleq \ln[(1 - \epsilon_1)/\epsilon_1]$. This approximation is accurate for small average error

probability ϵ_1 and the approximation error is biggest for $t = T_a$. We note that the diversity combiner resulting from this piecewise-linear approximation relates to the clipped-linear combiners in [11], where the basic idea is to limit the impact of partial-band interference by clipping the output of envelope detectors with respect to the signal output voltage. In our scenario, we limit the impact of uncertainty from the decisions of relay. Since the detector in [11] employs knowledge of the probability with which the interference appears, our approximations might provide a mechanism for optimizing the clipping level in that context as well. It is obvious that (3.5) is much simpler from the implementation point of view than (3.4) since, (3.5) only requires a comparison device rather than a nonlinear function $\ln(\cdot)$.

Now the PL detector is

$$t_0 + f_{PL}(t_1) \stackrel{0}{\underset{1}{\geq}} 0, \quad (3.6)$$

where t_0 and t_1 are the sufficient statistics output by the functions $g_0(y'_{01}, y'_{02})$ and $g_1(y'_{11}, y'_{12})$ respectively from (3.3).

Note that, conditioned on $x_0 = 0$, t_0 is the difference between two exponential random variables with rates λ_0 and λ'_0 , and t_1 is the difference between two exponential random variables with rates λ_1 and λ'_1 , where

$$\begin{aligned} \lambda_0 &= \frac{1}{\bar{\gamma}_{0,2}}, & \lambda'_0 &= 1 + \frac{1}{\bar{\gamma}_{0,2}}, \\ \lambda_1 &= \frac{1}{\bar{\gamma}_{1,2}}, & \lambda'_1 &= 1 + \frac{1}{\bar{\gamma}_{1,2}}. \end{aligned} \quad (3.7)$$

Moreover, t_0 and t_1 are conditionally independent given x_0 . Thus, after determining the probability density functions (pdf) of these two random variables, by applying the total probability law to (3.6) and performing the integral, we obtain the complicated, but closed-form, expression for the bit error probability

$$P_b = A_1 + A_2 + A_3, \quad (3.8)$$

where

$$\begin{aligned}
A_1 &= h(\lambda'_0, \lambda_0, -T_a) \times \{(1 - \epsilon_1) [1 - h(\lambda'_1, \lambda_1, T_a)] + \epsilon_1 [1 - h(\lambda_1, \lambda'_1, T_a)]\}, \\
A_2 &= h(\lambda'_0, \lambda_0, T_a) \times [(1 - \epsilon_1)h(\lambda'_1, \lambda_1, -T_a) + \epsilon_1 h(\lambda_1, \lambda'_1, -T_a)], \\
A_3 &= [q(\lambda'_0, \lambda_0, \lambda'_1, \lambda_1, -T_a) (1 - \epsilon_1) + q(\lambda'_0, \lambda_0, \lambda_1, \lambda'_1, -T_a) \epsilon_1] \times \\
&\quad \{[h(\lambda'_1, \lambda_1, 0) - h(\lambda'_1, \lambda_1, -T_a)] (1 - \epsilon_1) + [h(\lambda_1, \lambda'_1, 0) - h(\lambda_1, \lambda'_1, -T_a)] \epsilon_1\} \\
&\quad + [n(\lambda'_0, \lambda_0, \lambda'_1, \lambda_1, T_a) (1 - \epsilon_1) + n(\lambda'_0, \lambda_0, \lambda_1, \lambda'_1, T_a) \epsilon_1] \times \\
&\quad \{[h(\lambda'_1, \lambda_1, T_a) - h(\lambda'_1, \lambda_1, 0)] (1 - \epsilon_1) + [h(\lambda_1, \lambda'_1, T_a) - h(\lambda_1, \lambda'_1, 0)] \epsilon_1\}.
\end{aligned} \tag{3.9}$$

The functions in (3.9) are defined as follows,

$$h(r_0, r_1, t) \triangleq \begin{cases} 1 - \frac{r_0}{r_0 + r_1} e^{-r_1 t} & \text{for } t \geq 0 \\ \frac{r_1}{r_0 + r_1} e^{r_0 t} & \text{for } t \leq 0 \end{cases}, \tag{3.10}$$

$$q(r_1, r_2, r_3, r_4, t) \triangleq 1 - \frac{r_1 r_3}{(r_1 + r_2)(r_2 + r_3)} \cdot \frac{1 - e^{(r_2 + r_3)t}}{1 - e^{r_3 t}}, \tag{3.11}$$

$$n(r_1, r_2, r_3, r_4, t) \triangleq \frac{r_2 r_4}{(r_1 + r_2)(r_1 + r_4)} \cdot \frac{1 - e^{(r_1 + r_4)t}}{1 - e^{-r_4 t}}. \tag{3.12}$$

Some interpretations are provided here to help understand these involved expressions. Actually, A_1 is the probability of error for the PL detector given $t_1 \leq -T_a$, A_2 is the probability of error for the PL detector given $t_1 \geq T_a$, and A_3 is the probability of error for the PL detector given $-T_a \leq t_1 \leq T_a$. Note that $h(r_0, r_1, t)$ is actually the probability distribution function of the difference between two exponential random variables with parameters r_1 and r_0 , respectively. The tedious process to obtain these expressions is fully illustrated in Chapter 4 using the example of two parallel relays.

As we will see in the sequel, the error probability (3.8) of the PL detector using (3.5) provides a tight upper bound on the error probability of the nonlinear ML detector using (3.4) in all cases we consider. This observation suggests that we can use the much simpler (3.5) rather than the more complex (3.3) in the detector while maintaining the benefits of diversity. In Chapter 4, this technique has been extended to the cases in which the system has two parallel relays or has two antennas at the destination. The PL detector is also applicable to the coherent case as shown in Section 4.1.

3.2.3 High SNR Approximation

Although (3.8) provides a close approximation of the performance of noncoherent cooperative diversity with a decoding relay, it is too complicated to provide more insight about the system. Therefore, we develop an approximation of (3.8) suitable for high SNR. In high SNR regimes, the performance of cooperative diversity can be parameterized by the diversity order d and coding gain c , which are defined as follows,

$$\lim_{\bar{\gamma} \rightarrow \infty} P_b \bar{\gamma}^d = c. \quad (3.13)$$

Examining (3.7) and (3.8), we note that three SNRs, namely $\bar{\gamma}_{0,2}, \bar{\gamma}_{0,1}, \bar{\gamma}_{1,2}$, parameterize performance. Our high SNR approximation allows all three parameters to become large, but keeps them in fixed proportions to one another. This constraint of proportionality is for the purpose of accounting for the effect of network geometry on performance. Specifically, we assume

$$\bar{\gamma}_{0,2} = k_1 \bar{\gamma}, \quad \bar{\gamma}_{0,1} = k_2 \bar{\gamma}, \quad \bar{\gamma}_{1,2} = k_3 \bar{\gamma}, \quad (3.14)$$

where $\bar{\gamma}$ can be the average single-hop SNR and k_1, k_2, k_3 are constants related with the network geometry as well as the path loss model.

The following procedure describes how to obtain the high SNR approximation:

1. (3.14) is substituted into (3.7),
2. Express (3.8) as a function of $\frac{1}{\bar{\gamma}}, k_1, k_2, k_3$,
3. Take power series of (3.8) around the point $\frac{1}{\bar{\gamma}} = 0$. The first term of the series is regarded as an asymptotic approximation².

The result is

$$P_b \lesssim \frac{1}{\bar{\gamma}^2} \left(\frac{3}{k_1 k_3} + \frac{2 - \ln \frac{1}{k_2} + \ln \bar{\gamma}}{k_1 k_2} \right). \quad (3.15)$$

As we will see, (3.15) provides a very tight approximation to the simulation results as SNR becomes large. The geometric interpretation of (3.15) shows that there exists an asymmetry in the performance of noncoherent cooperative diversity. This is different from coherent cooperative diversity with an amplifying relay.

²This power series is done with the maple function *asympt*.

For coherent amplify-and-forward cooperative diversity [22], the BER for coherent amplify-and-forward cooperative diversity is shown to be $P'_b \approx \frac{1}{\bar{\gamma}^2} \frac{1}{k_1} \left(\frac{1}{k_2} + \frac{1}{k_3} \right)$, which indicates the optimum location for the amplifying relay is halfway between the source and destination. The asymmetry in (3.15) suggests the location for the noncoherent decoding relay to maximize the system performance might be different from that of coherent amplify-and-forward. Minimization of (3.15) given SNR values indicates that, for the path loss model assumed in this thesis, the optimal location for coherent amplify-and-forward is closed to the optimal position for noncoherent decode-and-forward.

However, the expression (3.15) demonstrates that cooperative diversity does not achieve full diversity order $d = 2$ for asymptotically high SNR since $\lim_{\bar{\gamma} \rightarrow \infty} P_b \bar{\gamma}^2 = \infty$ due to the existence of $\ln \bar{\gamma}$. This is contrary to what we might have expected since there are two conditionally independent channel inputs for cooperative diversity. It can be shown that

$$\ln \bar{\gamma} < \bar{\gamma}^\delta \quad \text{for} \quad \delta > 0. \quad (3.16)$$

Therefore, the diversity order for cooperative diversity can be expressed as $2 - \delta$. It can be arbitrarily close to 2, but never reaches 2. In Chapter 4, the analysis here is extended to cooperative diversity with two parallel decoding relays. It turns out that the diversity order obtained for cooperative diversity with two parallel decoding relays is 2 rather than 3. These surprising observations have motivated the following section in order to explain these unexpected results.

3.2.4 Analysis of Diversity Order for Cooperative Diversity with Multiple Relays

This section utilizes Bhattacharyya upper bound techniques to show that the diversity order for cooperative diversity with $M - 1$ parallel decoding relays is lower bounded by $1 + (M - 1)/2$. As there are only two codewords, namely $\mathbf{x}_0 = 0$ and $\mathbf{x}_0 = 1$, the pairwise error probability is equal to uncoded BER assuming equiprobable signals. The Bhattacharyya upper bound of the pairwise error probability between these two code words is

$$P_b \leq \prod_{i=0}^{M-1} \int_{y'_{i1}, y'_{i2}} \{p(y'_{i1}, y'_{i2} | \mathbf{x}_0 = 0)p(y'_{i1}, y'_{i2} | \mathbf{x}_0 = 1)\}^{1/2} dy'_{i1} dy'_{i2}, \quad (3.17)$$

where

$$p(y'_{i1}, y'_{i2} | x_0) = \begin{cases} \frac{\exp\left[-\frac{|y'_{01}|^2}{N_0 + E_0\sigma_{0,M}(1-x_0)}\right]}{\pi [N_0 + E_0\sigma_{0,M}(1-x_0)]} \frac{\exp\left[-\frac{|y'_{02}|^2}{N_0 + E_0\sigma_{0,M}(x_0)}\right]}{\pi [N_0 + E_0\sigma_{0,M}(x_0)]} & \text{for } i = 0 \\ \frac{\exp\left[-\frac{|y'_{i1}|^2}{N_0 + E_i\sigma_{i,M}(1-x_0)}\right]}{\pi [N_0 + E_i\sigma_{i,M}(1-x_0)]} \frac{\exp\left[-\frac{|y'_{i2}|^2}{N_0 + E_i\sigma_{i,M}(x_0)}\right]}{\pi [N_0 + E_i\sigma_{i,M}(x_0)]} (1 - \epsilon_i) & \text{otherwise} \\ + \frac{\exp\left[-\frac{|y'_{i1}|^2}{N_0 + E_i\sigma_{i,M}(x_0)}\right]}{\pi [N_0 + E_i\sigma_{i,M}(x_0)]} \frac{\exp\left[-\frac{|y'_{i2}|^2}{N_0 + E_i\sigma_{i,M}(1-x_0)}\right]}{\pi [N_0 + E_i\sigma_{i,M}(1-x_0)]} (\epsilon_i), & \end{cases} \quad (3.18)$$

where ϵ_i is the probability of error of relay R_i .

The difficulty of solving (3.17) lies in getting the terms outside the square root. Utilizing the Gaussian inequality, *i.e.*, $\sqrt{a+b+c} \leq \sqrt{a} + \sqrt{b} + \sqrt{c}$, it can be shown

$$P_b \leq \frac{4(1 + \bar{\gamma}_{0,M})}{(2 + \bar{\gamma}_{0,M})^2} \prod_{i=1}^{M-1} \left[\frac{4(1 + \bar{\gamma}_{i,M})}{(2 + \bar{\gamma}_{i,M})^2} \sqrt{2\epsilon_i^2 - 2\epsilon_i + 1} + 2\sqrt{\epsilon_i(1 - \epsilon_i)} \right]. \quad (3.19)$$

Assuming all relays are located at the same position, *i.e.*,

$$\bar{\gamma}_{0,M} = k_0\bar{\gamma}, \bar{\gamma}_{0,i} = k_2\bar{\gamma}, \bar{\gamma}_{i,M} = k_3\bar{\gamma}, \quad (3.20)$$

and $\epsilon_i = 1/(2 + \bar{\gamma}_{0,i})$ for $i = 1, \dots, M-1$, this upper bound at least has diversity order $1 + (M-1)/2$ since

$$\lim_{\bar{\gamma} \rightarrow \infty} P_b \bar{\gamma}^{1+(M-1)/2} \leq \frac{2^{M+1}}{k_1 k_2^{(M-1)/2}}, \quad (3.21)$$

if k_0, k_2, k_3 are nonzero constants. This lower bound of the diversity order is still valid when the relays are located in different positions as long as $\epsilon_i \propto 1/\bar{\gamma}_{0,i}$ and $\bar{\gamma}_{0,i} \propto \bar{\gamma}$ for asymptotically high SNR.

The trivial upper bound for the diversity order of cooperative diversity with $M-1$ relays can be M . This can be easily seen by assuming all relays are making right decisions, cooperative diversity becomes a M transmit antenna system, which is well known to have diversity order M . In summary, the diversity order for cooperative diversity with M decoding relays will satisfy

$$1 + (M-1)/2 \leq d \leq M. \quad (3.22)$$

This claim has been supported by the results from cooperative diversity with one or two decoding relays. As analyzed in Section 3.2.3, the diversity order for cooperative diversity with one decoding relay is less than 2. This clearly satisfies (3.22). Moreover, it is suggested in (3.22) that the diversity order should be higher than 1.5. This is verified to be true. From (4.15), it is clear that this claim is also true for cooperative diversity with two decoding relays with $M = 3$. Although the upper bound (3.19) is quite loose, it does not necessarily mean that this lower bound for diversity order is loose. The example of cooperative diversity with two decoding relays in Section 4.2 suggests this lower bound might be tight for multiple relays.

The bounds of diversity order (3.22) can be shown to apply to coherent cooperative diversity with decoding relays as well.

3.3 Numerical Results

The numerical simulation conditions in this chapter follow the same lines as in [14]. Specifically, the coordinates of the whole communication network are normalized by the distance $d_{0,2}$ between the source and destination transceivers, and the positive direction is defined as from source to destination. Without loss of generality, the source is assumed to be located at $(0, 0)$, and the destination located at $(1, 0)$. For simplicity of exposition, the relay is assumed to be located at $(\rho, 0)$. In general, the coordinates of the relay can be arbitrary. The fading variances $\sigma_{a_{i,j}}^2$ are assigned using a path-loss model in the form of $\sigma_{a_{i,j}}^2 \propto d_{i,j}^{-v}$, where $d_{i,j}$ is the distance from node i to node j , and v is a constant, chosen as 4 in our setup. The total network energy per transmitted bit is also normalized to 1. Specifically, we set $E_0 = 1$ for single-hop transmission; for diversity transmission, we assign equal sharing of power among the transmitters, *i.e.*, $E_0 = E_1 = 1/2$. We note that this power allocation does not consider the channel condition and need not be optimal in general.

Figs. 3.4–3.6 show simulated average bit-error rates for uncoded BFSK transmissions for relay locations $(0.1, 0)$, $(0.5, 0)$, and $(0.9, 0)$ respectively. They show that there is an apparent increase in slope on log scale for cooperative diversity in all three cases. This is the effect of the diversity gain. Furthermore, in Figs. 3.4–3.6, the curves for cooperative diversity transmission also demonstrate certain shifts to

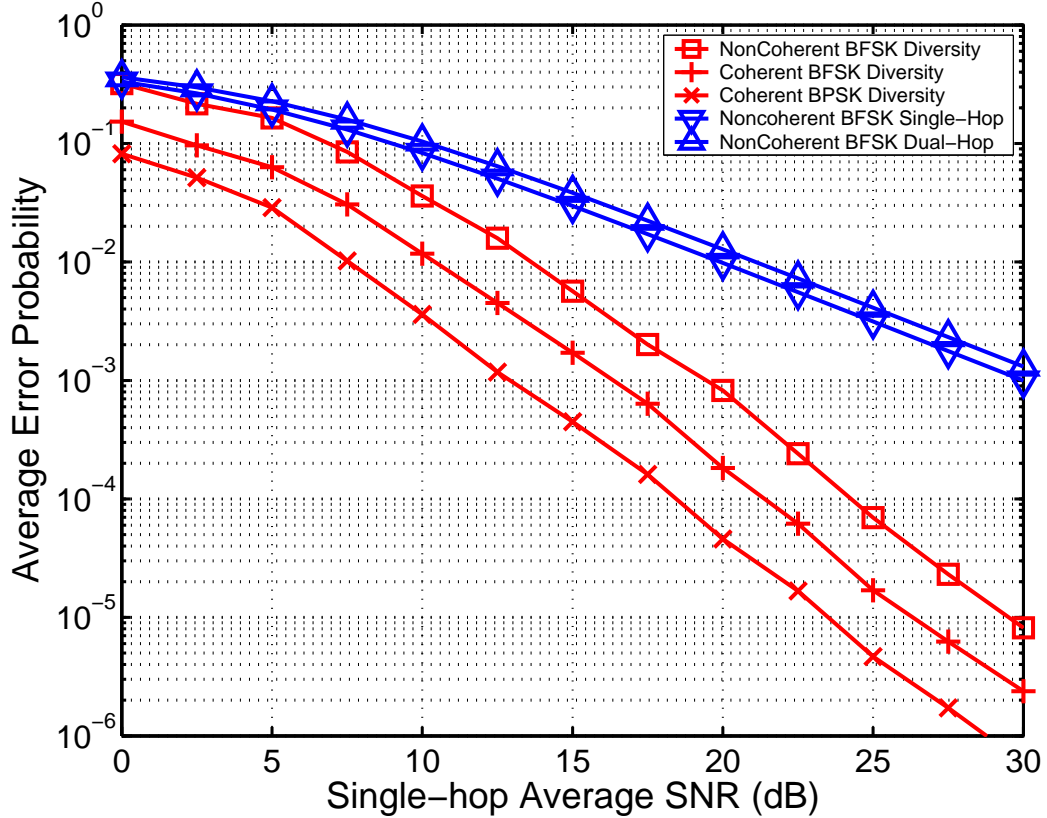


Figure 3.4. Error probability performance of cooperative diversity with a decoding relay located at $(0.1,0)$, *i.e.*, close to the source.

the left, which combats path-loss. These coding gains vary depending on the location of the relay. Optimizing the position of the relay to achieve the highest coding gain might be a key objective when the terminals want to form a cooperative group [22]. Among the three scenarios we simulated, cooperative diversity performs best when the relay is located halfway between the source and destination.

Simulation results for the average bit error rate for cooperative diversity with coherent BFSK and BPSK are also displayed in the plots. The shifts among the curves vary slightly with the position of the relay, though, in general, coherent BFSK is about 3 dB worse than BPSK, and about 3 dB better than noncoherent BFSK. As the error probability for coherent cooperative diversity with a decoding relay is not in closed-form, the closed-form (3.8) plus 3 dB will provide another type of approximation for the uncoded BER in coherent cooperative diversity with BFSK.

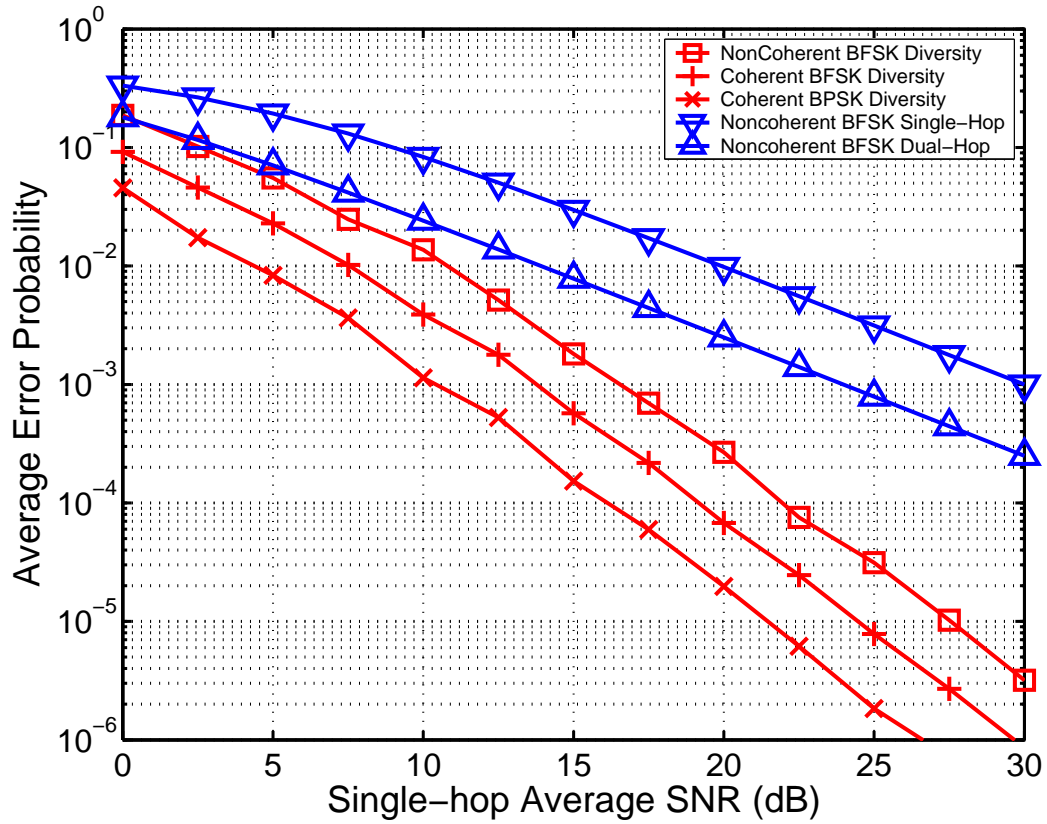


Figure 3.5. Error probability performance of cooperative diversity with a decoding relay located at $(0.5,0)$, *i.e.*, halfway between the source and destination.

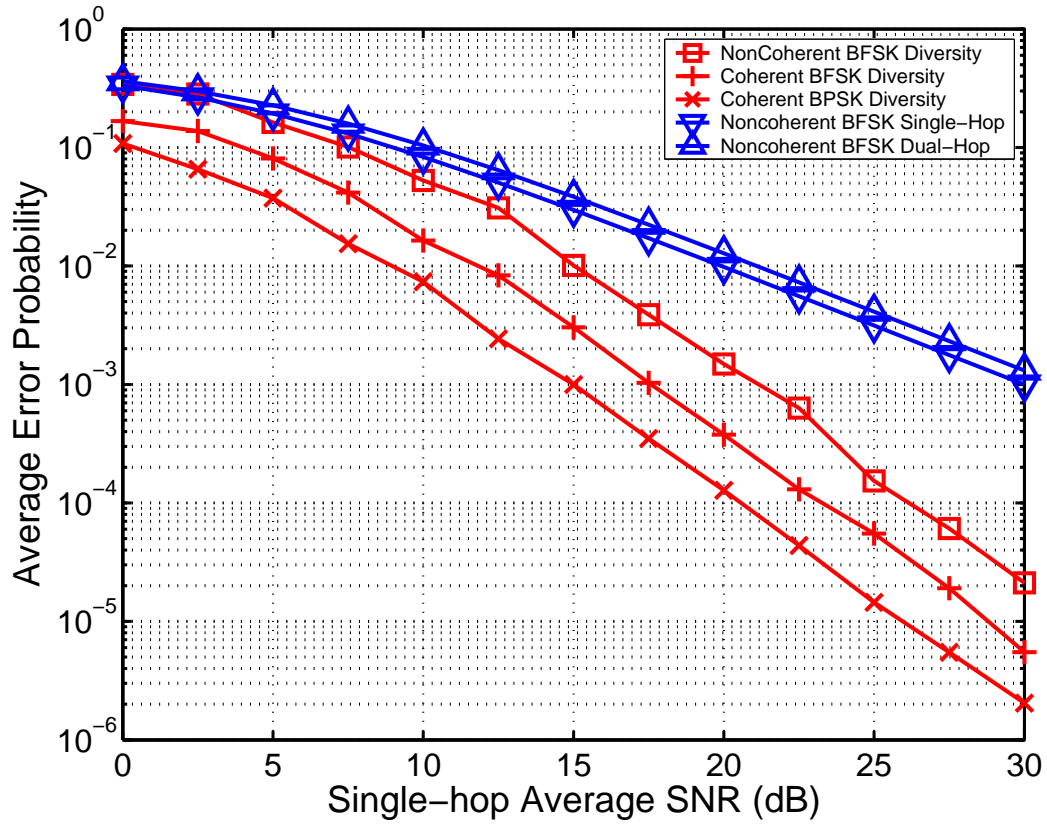


Figure 3.6. Error probability performance of cooperative diversity with a decoding relay located at $(0.9,0)$, *i.e.*, close to the destination.

Figs. 3.7–3.9 compare the results from PL approximation and high SNR approximation with simulation results for noncoherent cooperative diversity. The curves represented PL approximation overlap the simulation results of nonlinear ML detectors in all SNR regimes simulated here. Since the error probability of the PL detector is in closed-form and consists of only elementary functions, it is convenient for estimating performance of both the ML and PL detectors, rather than resorting to expensive Monte-Carlo simulations.

The curves for the high SNR approximations (3.15) are also presented in the plots. Note that $k_1 = \frac{1}{2}$, $k_2 = \frac{1}{2}d_{0,1}^{-4}$, $k_3 = \frac{1}{2}d_{1,2}^{-4}$ according to the path-model adopted in this paper, and $\bar{\gamma}$ is the average SNR for single hop transmission. In all scenarios, the curves for (3.15) begin to overlap with simulation results when SNR is higher than 15 dB.

3.4 Issues of Amplify-and-Forward in Noncoherent Cooperative Diversity

This chapter has so far focused on noncoherent cooperative diversity with a decode-and-forward protocol at the relay. This section explores the problem of amplify-and-forward protocol in noncoherent cooperative diversity. Analysis of the amplify-and-forward protocol becomes quite complicated in the case of noncoherent demodulation. To satisfy the power constraint without CSI greatly complicates the effort of obtaining a ML detector as well as evaluating its performance. This section focuses on the simple case of one relay to illustrate this point.

The matched filter outputs at the relay are

$$\begin{aligned} y_{11} &= (1 - x_0)\sqrt{E_0}a_{0,1} + n_{11}, \\ y_{12} &= x_0\sqrt{E_0}a_{0,1} + n_{12}, \end{aligned} \tag{3.23}$$

respectively. These signals are amplified by a factor of β at the relay before they are transmitted to the destination. To satisfy the power constraint at the relay, the amplifier gain β can be written as

$$\beta = \sqrt{\frac{E_1}{|y_{11}|^2 + |y_{12}|^2}}. \tag{3.24}$$

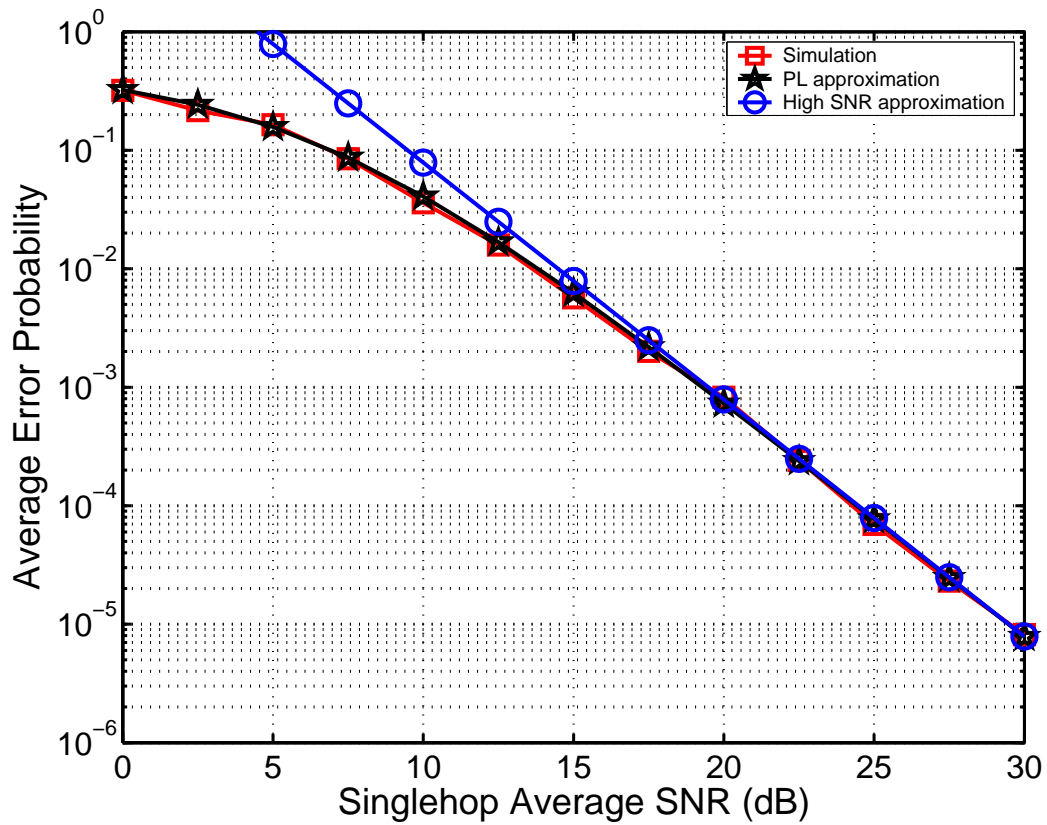


Figure 3.7. Compare the results from PL approximation and high SNR approximation with simulation results for noncoherent cooperative diversity with a decoding relay located at $(0.1,0)$, *i.e.*, close to the source.

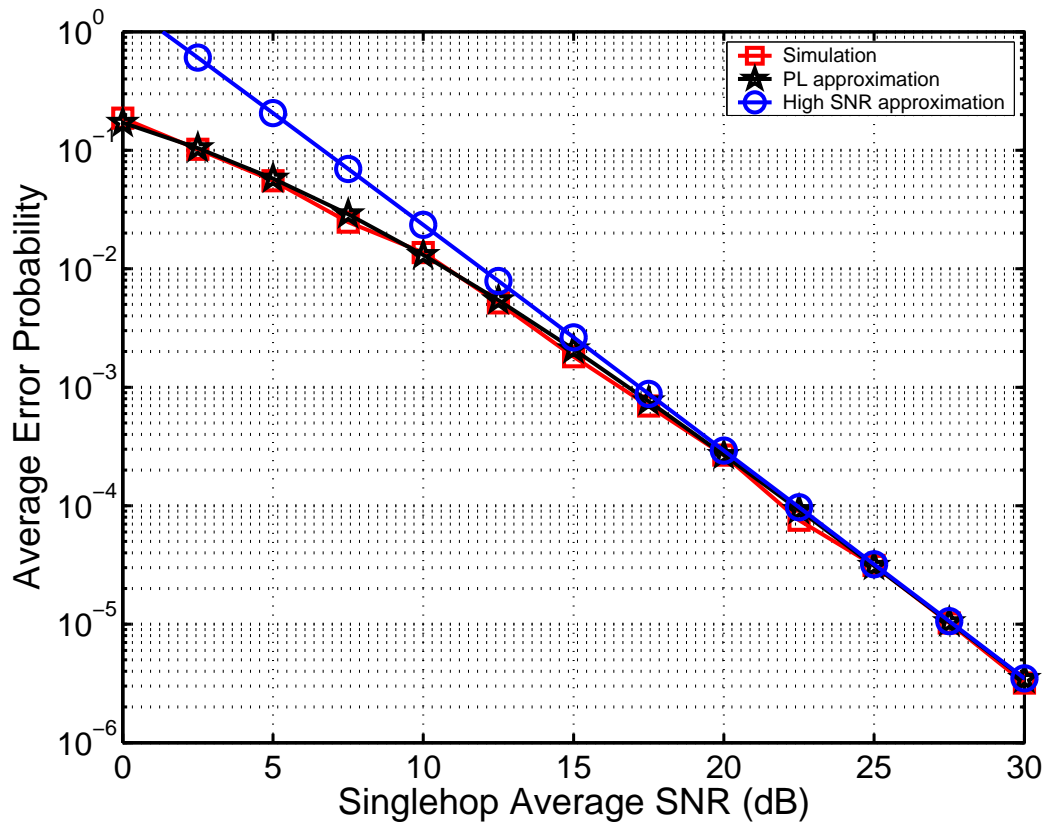


Figure 3.8. Compare the results from PL approximation and high SNR approximation with simulation results for noncoherent cooperative diversity with a decoding relay located at $(0.5,0)$, *i.e.*, halfway between the source and destination.

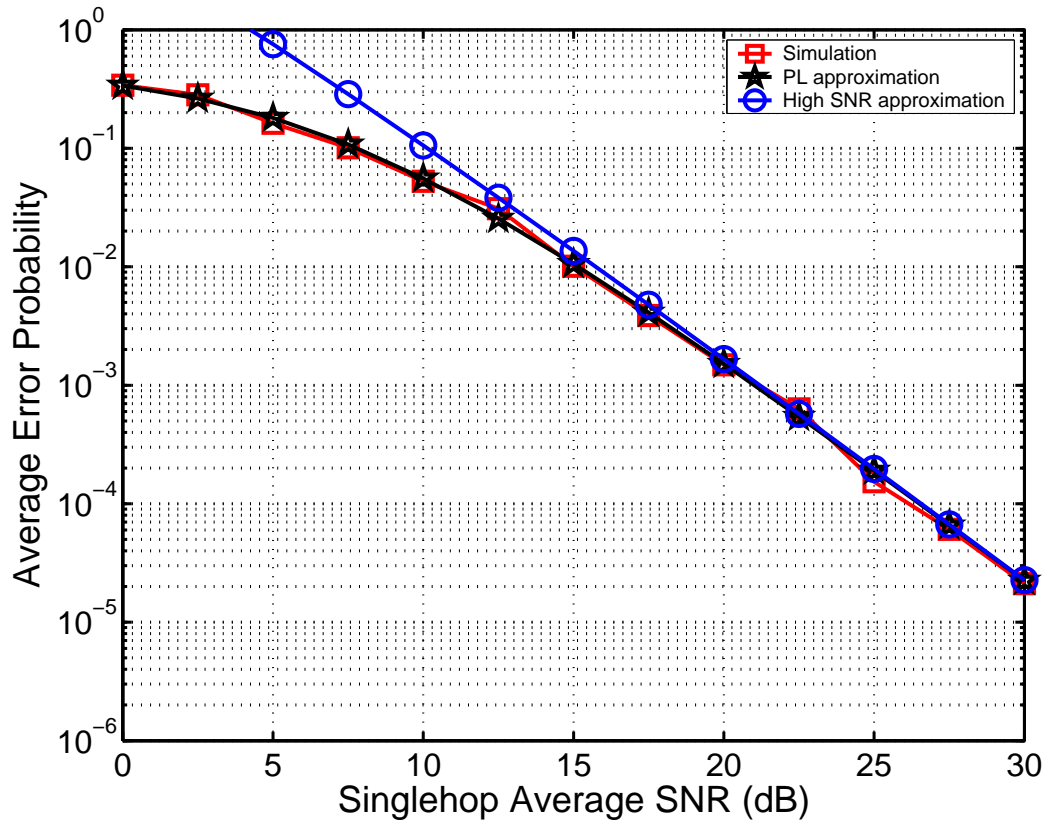


Figure 3.9. Compare the results from PL approximation and high SNR approximation with simulation results for noncoherent cooperative diversity with a decoding relay located at $(0.9,0)$, *i.e.*, close to the destination.

Thus, the matched filter outputs at the destination are

$$\begin{aligned} y'_{11} &= \beta y_{11} \mathbf{a}_{1,2} + n'_{11}, \\ y'_{12} &= \beta y_{12} \mathbf{a}_{1,2} + n'_{12}, \end{aligned} \quad (3.25)$$

respectively. The received signals y'_{11}, y'_{12} are conditionally independent given the corresponding fading coefficients, source symbols, and the amplifier gain. For non-coherent case in which the amplifier gain is unknown, y'_{11}, y'_{12} are correlated random variables given the source symbol x_0 . To obtain the joint pdf for the received signals, we define an auxiliary random variable as

$$s = \frac{|y_{11}|^2}{|y_{11}|^2 + |y_{12}|^2} \quad (3.26)$$

and express the received signals at destination as

$$\begin{aligned} y'_{11} &= \sqrt{E_1} s \mathbf{a}_{1,2} + n'_{11}, \\ y'_{12} &= \sqrt{E_1} \sqrt{1-s^2} \mathbf{a}_{1,2} + n'_{12}. \end{aligned} \quad (3.27)$$

To illustrate the challenge of obtaining the ML detector, we focus on getting the pdf of y'_{11}, y'_{12} given the signal $x_0 = 0$ is sent. Through some algebra, the pdf of the auxiliary random variable is

$$p_s(s|x_0 = 0) = \begin{cases} \frac{2cs}{((1-c)s^2+c)^2}, & \text{for } 0 \leq s \leq 1 \\ 0, & \text{otherwise} \end{cases}, \quad (3.28)$$

where $c = 1 + \bar{\gamma}_{0,1}$.

Noticing the received signals at the relay are conditionally independent Gaussian random variables given t, x_0 , the conditional pdf can be expressed as,

$$p(y'_{11}, y'_{12}|x_0 = 0, s = s) = \frac{1}{\pi^2 N_0 (N_0 + E_1 \sigma_{\mathbf{a}_{1,2}}^2)} \exp \left\{ \frac{A}{N_0 (N_0 + E_1 \sigma_{\mathbf{a}_{1,2}}^2)} \right\}, \quad (3.29)$$

with

$$\begin{aligned} A &= -|y'_{11}|^2 (N_0 + E_1 \sigma_{\mathbf{a}_{1,2}}^2) - y'_{12} N_0 + t^2 E_1 \sigma_{\mathbf{a}_{1,2}}^2 (|y'_{11}|^2 - |y'_{12}|^2) \\ &\quad + 2\text{Re}(y'_{12}^* y'_{11}) t \sqrt{1-t^2} E_1 \sigma_{\mathbf{a}_{1,2}}^2. \end{aligned} \quad (3.30)$$

Combining (3.29) and (3.28), the joint pdf of y'_{11}, y'_{12} given the signal $x_0 = 0$ can be evaluated as

$$p(y'_{11}, y'_{12} | x_0 = 0) = \int_s p(y'_{11}, y'_{12} | x_0 = 0, s = s) f_s(s | x_0 = 0) ds. \quad (3.31)$$

Unfortunately, this integral is quite complicated. Although numerical methods can be employed to evaluate this integral, the simulation still encounters significant difficulty. The reason is that the ML detector is

$$t_0 + \ln \frac{p(y'_{11}, y'_{12} | x_0 = 0)}{p(y'_{11}, y'_{12} | x_0 = 1)} \stackrel{0}{\underset{1}{\geq}} 0, \quad (3.32)$$

where t_0 is the sufficient statistics output from (3.3) for $i = 0$. The numerical values for the second term in (3.32), *i.e.*, $\ln \frac{p(y'_{11}, y'_{12} | x_0 = 0)}{p(y'_{11}, y'_{12} | x_0 = 1)} = \ln p(y'_{11}, y'_{12} | x_0 = 0) - \ln p(y'_{11}, y'_{12} | x_0 = 1)$, can be relatively large and have significant impact on decision making when both $p(y'_{11}, y'_{12} | x_0 = 0)$ and $p(y'_{11}, y'_{12} | x_0 = 1)$ are very small so that the numerical routines treat them as zeros. Therefore, more theoretical insights about (3.29) are needed in order to further simplify (3.32) to provide more precise simulation results for the noncoherent amplify-and-forward protocol.

The power constraint adopted here, *i.e.*

$$|\beta^2| (|y_{11}|^2 + |y_{12}|^2) \leq E_1, \quad (3.33)$$

can also apply to coherent scenarios. It is different with the power constraint normally adopted in the coherent case [14], *i.e.*,

$$|\beta^2| (E_0 |a_{0,1}|^2 + 2N_0) \leq E_1. \quad (3.34)$$

The difference between (3.33) and (3.34) is that (3.33) accounts for the instantaneous noise power and (3.34) focuses more on the average power of the AWGN. In this sense, (3.33) is more rigid than (3.34). It can be verified by simulation that, for coherent demodulation, there is no significant difference for these two different power constraints in terms of uncoded bit error rate, as long as the amplifier gain is available to the destination.

CHAPTER 4

EXTENSION OF PIECEWISE-LINEAR TECHNIQUES

Chapter 3 develops a piecewise-linear (PL) approximation to the nonlinear ML detectors for cooperative diversity with decode-and-forward protocol. This PL detector not only has some implementation advantages, but also leads to a closed-form approximation for uncoded BER in noncoherent cooperative diversity with a decoding relay. This chapter further extends the PL techniques to three other cases, namely coherent cooperative diversity with a decoding relay, noncoherent cooperative diversity with two relays and noncoherent cooperative diversity with two receive antennas at the destination. The first example shows that the PL detector is not only useful for noncoherent cooperative diversity, but also applicable to coherent cooperative diversity. The uncoded BER based on the PL detector for coherent cooperative diversity with a decoding relay is expressed as an integral, and provides a tight approximation of the simulation results with nonlinear ML detectors. The second example serves the purpose of demonstrating the power and restriction of the PL techniques in the case of multiple relays. It also provides an opportunity of examining performance for cooperative diversity with two relays. The third example shows the flexibility of the general detector structure proposed in Chapter 3 as it can be modified to accommodate the ML detector for cooperative diversity with two antennas at the destination. It also shows the importance of the PL approximation and verifies that cooperative diversity can be exploited together with spatial diversity brought by multiple antennas at the destination.

4.1 Coherent Cooperative Diversity with the Piecewise-Linear Detector

This section investigates the performance of the coherent demodulation with a decoding relay. To facilitate the comparison between the coherent and noncoherent cases, we again focus on BFSK. The extension to BPSK, another common coherent modulation scheme, is straightforward. In this section, the PL approximation technique of Section 3.2.2 is extended to the case of coherent demodulation. Although coherent modulation and demodulation for cooperative diversity has been extensively investigated in [14, 22, 6], little attention has been paid to coherent decode-and-forward. An upper bound provided for coherent decode-and-forward in [14] is only tight when the relay is close to the source.

Assuming the destination knows the average error probability ϵ_1 at the relay, the coherent ML detector can be employed as shown in Fig. 3.2 by using functions,

$$g_i(y'_{i1}, y'_{i2}) = \frac{2 (\operatorname{Re}\{y'_{i1} \mathbf{a}_{i,2}^*\} - \operatorname{Re}\{y'_{i2} \mathbf{a}_{i,2}^*\}) \sqrt{E_i}}{N_0} \quad (4.1)$$

for $i = 0, 1$, and $f_1(\mathbf{t}_1)$ as in (3.4). The superscript $*$ denotes the conjugate. This detector can be further simplified to the detector structure in [14].

Using the piecewise-linear detector and following steps similar to the noncoherent case, the error probability conditional on the instantaneous SNR is

$$\begin{aligned} P_{b|\gamma_{0,2}, \gamma_{1,2}} = & \left[1 - Q \left(\frac{T_a - 2\gamma_{0,2}}{\sqrt{4\gamma_{0,2}}} \right) \right] \times \\ & \left[1 - (1 - \epsilon_1) Q \left(\frac{-T_a - 2\gamma_{1,2}}{\sqrt{4\gamma_{1,2}}} \right) - \epsilon_1 Q \left(\frac{-T_a + 2\gamma_{1,2}}{\sqrt{4\gamma_{1,2}}} \right) \right] \\ & + \left[1 - Q \left(\frac{-T_a - 2\gamma_{0,2}}{\sqrt{4\gamma_{0,2}}} \right) \right] \times \\ & \left[(1 - \epsilon_1) Q \left(\frac{T_a - 2\gamma_{1,2}}{\sqrt{4\gamma_{1,2}}} \right) + \epsilon_1 Q \left(\frac{-T_a + 2\gamma_{1,2}}{\sqrt{4\gamma_{1,2}}} \right) \right] \\ & + \int_{-T_a}^{T_a} \left[\frac{1 - \epsilon_1}{\sqrt{8\pi\gamma_{1,2}}} \exp \left(-\frac{(t - 2\gamma_{1,2})^2}{8\gamma_{1,2}} \right) + \frac{\epsilon_1}{\sqrt{8\pi\gamma_{1,2}}} \exp \left(-\frac{(t + 2\gamma_{1,2})^2}{8\gamma_{1,2}} \right) \right] \\ & \times \left[1 - Q \left(\frac{-t - 2\gamma_{0,2}}{\sqrt{4\gamma_{0,2}}} \right) \right] dt, \end{aligned} \quad (4.2)$$

where $\epsilon_1 = \frac{1}{2} \left(1 - \sqrt{\frac{\bar{\gamma}_{0,1}}{2 + \bar{\gamma}_{0,1}}} \right)$ and $T_a = \ln \left(\frac{1 - \epsilon_1}{\epsilon_1} \right)$. For the Rayleigh fading assumption, the SNRs are exponentially distributed with average SNR as the parameter, *i.e.*, $p(\gamma_{0,2}) = \frac{e^{-\gamma_{0,2}/\bar{\gamma}_{0,2}}}{\bar{\gamma}_{0,2}}$ and $p(\gamma_{1,2}) = \frac{e^{-\gamma_{1,2}/\bar{\gamma}_{1,2}}}{\bar{\gamma}_{1,2}}$. Unfortunately, it turns out that the averaging of (4.2) with respect to the instantaneous SNRs is very involved and must be done numerically.

Simulation results for coherent cooperative diversity with a decoding relay is presented in Figs 4.1– 4.3. The simulation conditions for Figs 4.1– 4.3 follow the same line as in Chapter 3. The overlapping of curves for simulation results and numerical averaging results of (4.2) with respect to the distribution of $\gamma_{1,2}$ and $\gamma_{0,2}$ shows that results using PL detectors provide a very accurate approximation of the performance of ML detection for coherent cooperative diversity with a decoding relay. Therefore, the PL detector is also applicable to coherent cooperative diversity with decoding relays. It can also be observed from the plots that noncoherent BFSK loses about 3 dB compared to coherent BFSK in cooperative diversity. This conclusion is the same as in single-hop communication. Since we do not have a closed-form expression for the BER of coherent cooperative diversity, the curve for (3.8) plus 3 dB gain might provide another approximation to coherent cooperative diversity with decode-and-forward.

4.2 Noncoherent Cooperative Diversity with Two Decoding Relays

In this section, we provide a detailed derivation of the uncoded BER for cooperative diversity with two decoding relays by using the PL detectors introduced at Chapter 3. The derivation provides more insight about the techniques as well as the difficulty in extending the analysis of Section 3.2 to multiple relays based on piecewise-linear approximation.

Applying the total probability law and piecewise-linear approximation to the case of two parallel decoding relays, it is easy to see that the uncoded BER based

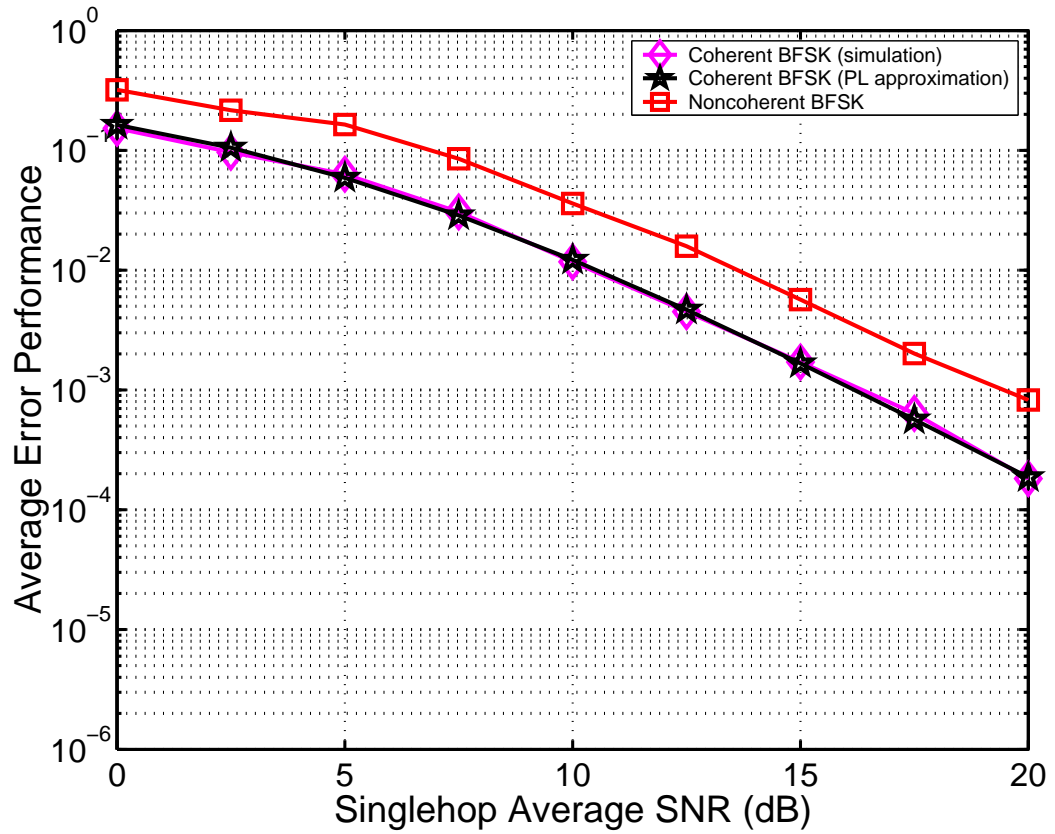


Figure 4.1. Error probability of coherent BFSK with the decoding relay located at $(0.1,0)$, i.e., close to the source.

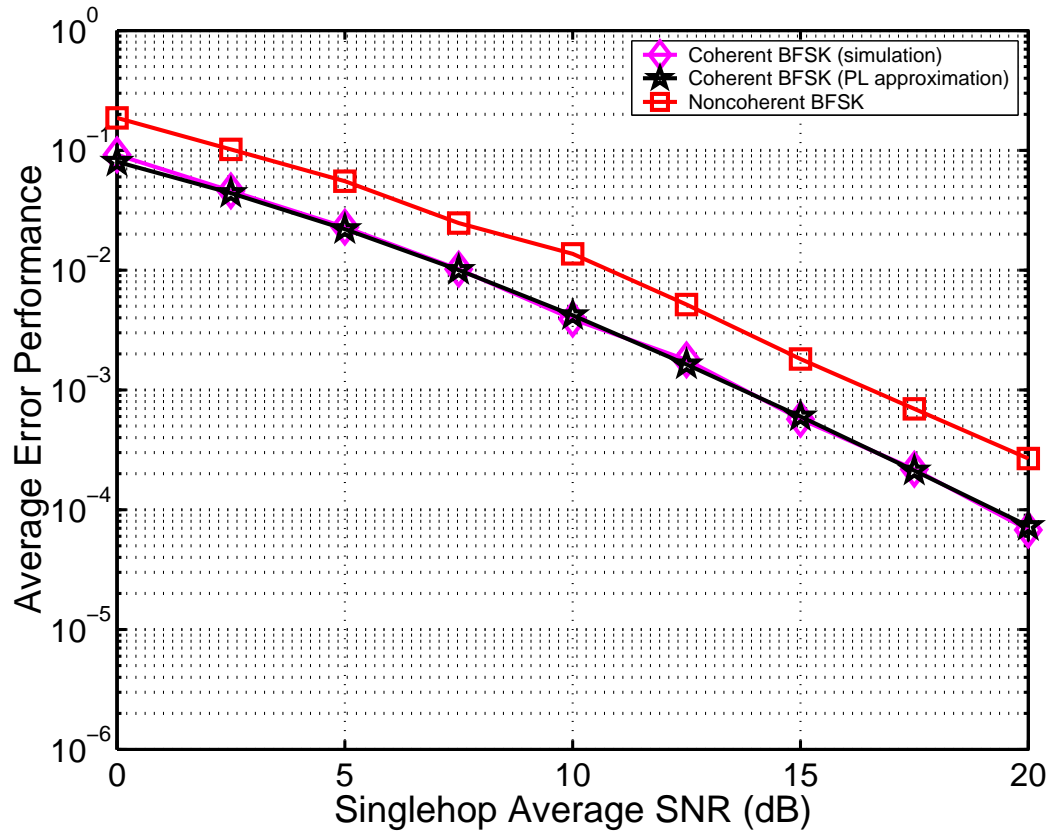


Figure 4.2. Error probability performance of coherent BFSK with the decoding relay located at (0.5,0), i.e., in the middle of source and destination.

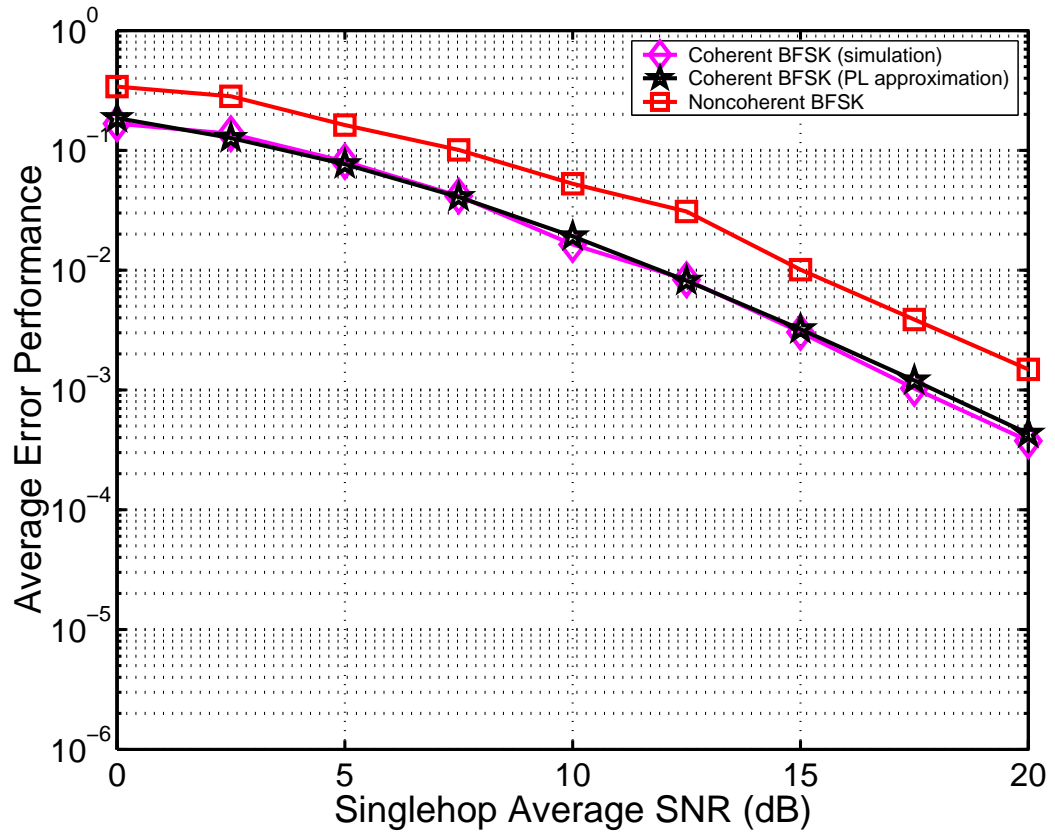


Figure 4.3. Error probability performance of coherent BFSK with the decoding relay located at $(0.9,0)$, i.e., close to the destination.

on PL approximation is

$$\begin{aligned}
P_b &= \Pr(\mathbf{t}_0 - T_{a1} - T_{a2} < 0 | \mathbf{x}_0 = 0) \Pr(\mathbf{t}_1 \leq -T_{a1} | \mathbf{x}_0 = 0) \Pr(\mathbf{t}_2 \leq -T_{a2} | \mathbf{x}_0 = 0) \\
&+ \Pr(\mathbf{t}_0 - T_{a1} + T_{a2} < 0 | \mathbf{x}_0 = 0) \Pr(\mathbf{t}_1 \leq -T_{a1} | \mathbf{x}_0 = 0) \Pr(\mathbf{t}_2 \geq T_{a2} | \mathbf{x}_0 = 0) \\
&+ \Pr(\mathbf{t}_0 + T_{a1} - T_{a2} < 0 | \mathbf{x}_0 = 0) \Pr(\mathbf{t}_1 \geq T_{a1} | \mathbf{x}_0 = 0) \Pr(\mathbf{t}_2 \leq -T_{a2} | \mathbf{x}_0 = 0) \\
&+ \Pr(\mathbf{t}_0 + T_{a1} + T_{a2} < 0 | \mathbf{x}_0 = 0) \Pr(\mathbf{t}_1 \geq T_{a1} | \mathbf{x}_0 = 0) \Pr(\mathbf{t}_2 \geq T_{a2} | \mathbf{x}_0 = 0) \\
&+ \Pr(\mathbf{t}_0 + \mathbf{t}_1 - T_{a2} < 0, -T_{a1} \leq \mathbf{t}_1 \leq T_{a1} | \mathbf{x}_0 = 0) \Pr(\mathbf{t}_2 \leq -T_{a2} | \mathbf{x}_0 = 0) \\
&+ \Pr(\mathbf{t}_0 + \mathbf{t}_1 + T_{a2} < 0, -T_{a1} \leq \mathbf{t}_1 \leq T_{a1} | \mathbf{x}_0 = 0) \Pr(\mathbf{t}_2 \geq T_{a2} | \mathbf{x}_0 = 0) \\
&+ \Pr(\mathbf{t}_0 + \mathbf{t}_2 - T_{a1} < 0, -T_{a2} \leq \mathbf{t}_2 \leq T_{a2} | \mathbf{x}_0 = 0) \Pr(\mathbf{t}_1 \leq -T_{a1} | \mathbf{x}_0 = 0) \\
&+ \Pr(\mathbf{t}_0 + \mathbf{t}_2 + T_{a1} < 0, -T_{a2} \leq \mathbf{t}_2 \leq T_{a2} | \mathbf{x}_0 = 0) \Pr(\mathbf{t}_1 \geq T_{a1} | \mathbf{x}_0 = 0) \\
&+ \Pr(\mathbf{t}_0 + \mathbf{t}_1 + \mathbf{t}_2 < 0, -T_{a1} \leq \mathbf{t}_1 \leq T_{a1}, -T_{a2} \leq \mathbf{t}_2 \leq T_{a2} | \mathbf{x}_0 = 0).
\end{aligned} \tag{4.3}$$

where

$$T_{ai} = \ln \left(\frac{1 - \epsilon_i}{\epsilon_i} \right) \tag{4.4}$$

for $i = 1, 2$.

To proceed, we need the following preliminary results. Suppose $\mathbf{x}_1, \mathbf{x}_2$ are independent exponential random variable with distribution $p(\mathbf{x}_1) = r_1 e^{-r_1 \mathbf{x}_1}$ and $p(\mathbf{x}_2) = r_2 e^{-r_2 \mathbf{x}_2}$, respectively. Defining $\mathbf{y} = \mathbf{x}_2 - \mathbf{x}_1$, it can be shown that the pdf of \mathbf{y} is

$$p(\mathbf{y}) = \begin{cases} \frac{r_1 r_2}{r_1 + r_2} e^{-r_2 \mathbf{y}} & \text{for } \mathbf{y} \geq 0 \\ \frac{r_1 r_2}{r_1 + r_2} e^{r_1 \mathbf{y}} & \text{for } \mathbf{y} \leq 0 \end{cases}, \tag{4.5}$$

and its cdf is

$$\Pr(\mathbf{y} \leq y) = h(r_1, r_2, y) = \begin{cases} 1 - \frac{r_1}{r_1 + r_2} e^{-r_2 y} & \text{for } y \geq 0 \\ \frac{r_2}{r_1 + r_2} e^{r_1 y} & \text{for } y \leq 0 \end{cases}. \tag{4.6}$$

Given $\mathbf{x}_0 = 0$ and the decision of relays, the distribution function of the sufficient statistics $\mathbf{t}_0, \mathbf{t}_1, \mathbf{t}_2$ are essentially the same with different parameters. And the different assumptions of the decision of relays will also result in the same distribution

function with a switching of parameters. This observation can further be illustrated by taking t_1 as an example. We have $t_1 = \frac{E_1\sigma_{a_1,2}^2}{(E_1\sigma_{a_1,2}^2+N_0)N_0} |y'_{11}|^2 - \frac{E_1\sigma_{a_1,2}^2}{(E_1\sigma_{a_1,2}^2+N_0)N_0} |y'_{12}|^2$. Given relay R_1 makes the right decision, both terms in t_1 are exponential random variables with $r_2 = \frac{1}{\bar{\gamma}_{0,1}}$ and $r_1 = 1 + \frac{1}{\bar{\gamma}_{0,1}}$. If relay R_1 is wrong, they are still exponential random variables with a switching of parameters, *i.e.*, $r_1 = \frac{1}{\bar{\gamma}_{0,1}}$ and $r_2 = 1 + \frac{1}{\bar{\gamma}_{0,1}}$. Therefore, the effort can be focused on the case in which all relays are right, the expression of probability of error obtained in this way can then be extended to other cases by switching the suitable parameters. This observation can greatly simplify the derivation. We denote the event that relay R_i makes the right decision as \mathcal{R}_i , the event that it makes the wrong decision as $\bar{\mathcal{R}}_i$.

Another observation to further simplify the derivation is to notice that the eight terms among (4.3) can be classified as three basic types, *i.e.*, terms including the probability of a single random variable, terms including the joint probability of two random variables and the last term including the joint probability of three random variables. Specifically, the first four terms in (4.3) only requires the individual distribution of t_0, t_1, t_2 , the following four terms in (4.3) requires the distribution of $t_0 + t_1$ and $t_0 + t_2$, and the last term requires the distribution of $t_0 + t_1 + t_2$.

In the following, we define the following parameter to facilitate the expression,

$$\begin{aligned}\lambda_i &= 1 + \frac{1}{\bar{\gamma}_{i,3}} \\ \lambda'_i &= \frac{1}{\bar{\gamma}_{i,3}},\end{aligned}\tag{4.7}$$

for $i = 0, 1, 2$. Note that here $i = 0$ denotes the source, $i = 1, 2$ denote the two relays and the subscript 3 denotes the destination.

It is easy to see that the first four terms in (4.3) can be expressed by using function (4.6). The general form for the following four terms of (4.3) can be expressed as

$$\begin{aligned}\Pr(t_0 + t_1 - S_b < 0, -S_a \leq t_1 \leq S_a | \mathcal{R}_1, x_0 = 0) &= \\ \int_{t_1=-S_a}^{S_a} p(t_1 | \mathcal{R}_1, x_1 = 0) \int_{t_0=-\infty}^{S_b-t_1} p(t_0 | \mathcal{R}_1, x_0 = 0) dt_0 dt_1\end{aligned}\tag{4.8}$$

From (4.5), the pdfs of $p(t_1 | \mathcal{R}_1, x_1 = 0)$ and $p(t_0 | \mathcal{R}_1, x_0 = 0)$ are different in positive and negative region, therefore different integration paths have to be taken

according to the different values of S_a, S_b . Through some tedious algebra, the result is,

$$\begin{aligned}
& \Pr(t_0 + t_1 - S_b < 0, -S_a \leq t_1 \leq S_a | \mathcal{R}_1, x_0 = 0) = m(\lambda_0, \lambda'_0, \lambda_1, \lambda'_1, S_a, S_b) \\
& = \begin{cases}
\begin{aligned}
& h(\lambda_1, \lambda'_1, S_a) - h(\lambda_1, \lambda'_1, -S_a) \\
& - \frac{\lambda_0 \lambda_1 \lambda'_1 e^{-\lambda'_0 T_{a2}}}{(\lambda_0 + \lambda'_0)(\lambda_1 + \lambda'_1)} \left[\frac{1 - e^{-(\lambda_1 + \lambda'_0) S_a}}{(\lambda_1 + \lambda'_0)} \right. \\
& \left. + \frac{e^{-(\lambda'_0 - \lambda'_1) S_a} - 1}{(\lambda'_0 - \lambda'_1)} \right] \qquad \text{for } S_b \geq S_a \geq 0
\end{aligned} \\
\begin{aligned}
& h(\lambda_1, \lambda'_1, S_b) - h(\lambda_1, \lambda'_1, -S_a) \\
& - \frac{\lambda_0 \lambda_1 \lambda'_1 e^{-\lambda'_0 T_{a2}}}{(\lambda_0 + \lambda'_0)(\lambda_1 + \lambda'_1)} \left[\frac{1 - e^{-(\lambda_1 + \lambda'_0) S_a}}{(\lambda_1 + \lambda'_0)} \right. \\
& \left. + \frac{e^{-(\lambda'_0 - \lambda'_1) S_b} - 1}{(\lambda'_0 - \lambda'_1)} \right] + \frac{\lambda_0 \lambda_1 \lambda'_1 e^{-\lambda_0 T_{a2}}}{(\lambda_0 + \lambda'_0)(\lambda_1 + \lambda'_1)(\lambda_0 + \lambda'_1)} \qquad \text{for } 0 \leq S_b \leq S_a \\
& \times \left[e^{-(\lambda_0 + \lambda'_1) S_b} - e^{-(\lambda_0 + \lambda'_1) S_a} \right] \\
\begin{aligned}
& h(\lambda_1, \lambda'_1, S_b) - h(\lambda_1, \lambda'_1, -S_a) \\
& - \frac{\lambda'_0 \lambda_1 \lambda'_1 e^{-\lambda'_0 T_{a2}}}{(\lambda_0 + \lambda'_0)(\lambda_1 + \lambda'_1)(\lambda_0 + \lambda'_1)} \left[e^{(\lambda_1 + \lambda'_0) S_b} \right. \\
& \left. - e^{-(\lambda_1 + \lambda'_0) S_a} \right] + \frac{\lambda'_0 \lambda_1 \lambda'_1 e^{\lambda_0 T_{a2}}}{(\lambda_0 + \lambda'_0)(\lambda_1 + \lambda'_1)} \\
& \times \left[\frac{1 - e^{-(\lambda_1 - \lambda_0) S_b}}{(\lambda_1 - \lambda_0)} + \frac{e^{-(\lambda'_1 + \lambda_0) S_a} - 1}{(\lambda'_1 + \lambda_0)} \right] \qquad \text{for } -S_a \leq S_b \leq 0 \\
\begin{aligned}
& \frac{\lambda'_0 \lambda_1 \lambda'_1 e^{\lambda_0 T_{a2}}}{(\lambda_0 + \lambda'_0)(\lambda_1 + \lambda'_1)} \left[\frac{1 - e^{-(\lambda_1 - \lambda_0) S_a}}{(\lambda_1 - \lambda_0)} \right. \\
& \left. + \frac{e^{-(\lambda'_1 + \lambda_0) S_a} - 1}{(\lambda'_1 + \lambda_0)} \right] \qquad \text{for } S_b \leq -S_a \leq 0
\end{aligned}
\end{cases} \tag{4.9}
\end{aligned}$$

The complexity of (4.9) mainly comes from the asymmetry of the pdf (4.5). This asymmetry makes the computation of the last term in (4.3),

$$\begin{aligned}
& \Pr(t_0 + t_1 + t_1 < 0, -T_{a1} \leq t_1 \leq T_{a1}, -T_{a2} \leq t_2 \leq T_{a2} | \mathcal{R}_1, \mathcal{R}_2, x_0 = 0) = \\
& \int_{t_1 = -T_{a1}}^{T_{a1}} p(t_1 | x_1 = 0) \int_{t_2 = -T_{a2}}^{T_{a2}} p(t_2 | x_2 = 0) \int_{t_0 = -\infty}^{-(t_1 + t_2)} p(t_0 | x_0 = 0) dt_0 dt_1 dt_2, \tag{4.10}
\end{aligned}$$

extremely difficult. As demonstrated above, a general expression can be obtained by separating the integration region step by step: first according to whether $t_1 + t_2$ is positive, then the relative values of t_1 and t_2 and then T_{a1} and T_{a2} . To simplify the derivation, it is assumed in the following that $T_{a1} = T_{a2}$, which means both relays are located at positions with the same distance from the source. This is the bottle neck of the expressions provided in the following,

$$\begin{aligned}
& \Pr(t_0 + t_1 + t_1 < 0, -T_{a1} \leq t_1 \leq T_{a1}, -T_{a2} \leq t_2 \leq T_{a2}, t_1 + t_2 \leq 0 | \mathcal{R}_1, \mathcal{R}_2, x_0 = 0) \\
& = n_1(\lambda_0, \lambda'_0, \lambda_1, \lambda'_1, \lambda_2, \lambda'_2, T_{a1}, T_{a2}) \\
& = [h(\lambda_1, \lambda'_1, 0) - h(\lambda_1, \lambda'_1, -T_{a1})] [h(\lambda_2, \lambda'_2, 0) - h(\lambda_2, \lambda'_2, -T_{a2})] \\
& \quad - \frac{\lambda_0 \lambda_1 \lambda'_1 \lambda_2 \lambda'_2}{(\lambda_0 + \lambda'_0)(\lambda_1 + \lambda'_1)(\lambda_2 + \lambda'_2)} \left[\frac{1 - e^{-(\lambda_2 + \lambda'_0)T_{a2}}}{\lambda_2 + \lambda'_0} \right] \left[\frac{1 - e^{-(\lambda_1 + \lambda'_0)T_{a2}}}{\lambda_1 + \lambda'_0} \right] \\
& \quad + \frac{\lambda'_1 \lambda_2 \lambda'_2}{(\lambda_1 + \lambda'_1)(\lambda_2 + \lambda'_2)} \left[\frac{1 - e^{-(\lambda_1 + \lambda'_2)T_{a1}}}{\lambda_1 + \lambda'_2} + \frac{e^{-\lambda_1 T_{a1}} (e^{-\lambda'_2 T_{a2}} - 1)}{\lambda_2} \right] \\
& \quad - \frac{\lambda'_1 \lambda_2 \lambda'_2}{(\lambda_1 + \lambda'_1)(\lambda_2 + \lambda'_2)} \frac{\lambda_0 \lambda_1}{(\lambda_0 + \lambda'_0)(\lambda_1 + \lambda'_0)} \left[\frac{1 - e^{-(\lambda_1 + \lambda'_2)T_{a1}}}{\lambda_1 + \lambda'_2} \right. \\
& \quad \left. - \frac{e^{-(\lambda'_0 + \lambda_1)T_{a1}} (e^{(\lambda'_0 - \lambda'_2)T_{a2}} - 1)}{\lambda'_0 - \lambda'_2} \right] + \frac{\lambda_1 \lambda'_1 \lambda_2 \lambda'_2}{(\lambda_1 + \lambda'_1)(\lambda_2 + \lambda'_2)} \left[\frac{1 - e^{-\lambda_2 T_{a2}}}{\lambda_2 \lambda'_1} \right. \\
& \quad \left. - \frac{1 - e^{-(\lambda'_1 + \lambda_2)T_{a2}}}{\lambda'_1 (\lambda_2 + \lambda'_1)} \right] - \frac{\lambda_0 \lambda_1 \lambda'_1 \lambda_2 \lambda'_2}{(\lambda_0 + \lambda'_0)(\lambda_1 + \lambda'_1)(\lambda_2 + \lambda'_2)} \times \\
& \quad \frac{1}{(\lambda'_0 - \lambda'_1)} \left[\frac{1 - e^{-(\lambda_2 + \lambda'_1)T_{a2}}}{\lambda_2 + \lambda'_1} - \frac{1 - e^{-(\lambda_2 + \lambda'_0)T_{a2}}}{\lambda_2 + \lambda'_0} \right]
\end{aligned} \tag{4.11}$$

and

$$\begin{aligned}
& \Pr(\mathbf{t}_0 + \mathbf{t}_1 + \mathbf{t}_1 < 0, -T_{a1} \leq \mathbf{t}_1 \leq T_{a1}, -T_{a2} \leq \mathbf{t}_2 \leq T_{a2}, \mathbf{t}_1 + \mathbf{t}_2 \geq 0 | \mathcal{R}_1, \mathcal{R}_2, \mathbf{x}_0 = 0) \\
& = n_2(\lambda_0, \lambda'_0, \lambda_1, \lambda'_1, \lambda_2, \lambda'_2, T_{a1}, T_{a2}) \\
& = \frac{\lambda_0 \lambda_1 \lambda'_1 \lambda_2 \lambda'_2}{(\lambda_0 + \lambda'_0)(\lambda_1 + \lambda'_1)(\lambda_2 + \lambda'_2)} \times \\
& \quad \frac{1}{\lambda_0 + \lambda'_1} \left[\frac{1 - e^{-(\lambda_2 + \lambda'_1)T_{a2}}}{\lambda_2 + \lambda'_1} - e^{-(\lambda_0 + \lambda'_1)T_{a2}} \frac{1 - e^{-(\lambda_2 - \lambda_0)T_{a2}}}{\lambda_2 - \lambda_0} \right] \\
& \quad + \frac{\lambda_0 \lambda_1 \lambda'_1 \lambda_2 \lambda'_2}{(\lambda_0 + \lambda'_0)(\lambda_1 + \lambda'_1)(\lambda_2 + \lambda'_2)} \frac{1}{\lambda_1 - \lambda_0} \left[\frac{1 - e^{-(\lambda_0 + \lambda'_2)T_{a2}}}{\lambda_0 + \lambda'_2} + \frac{e^{-(\lambda_1 - \lambda'_2)T_{a2}} - 1}{\lambda_1 - \lambda'_2} \right] \\
& \quad + \frac{\lambda_0 \lambda_1 \lambda'_1 \lambda_2 \lambda'_2}{(\lambda_0 + \lambda'_0)(\lambda_1 + \lambda'_1)(\lambda_2 + \lambda'_2)} \frac{1 - e^{-(\lambda_0 + \lambda'_1)T_{a1}}}{\lambda_0 + \lambda'_1} \frac{1 - e^{-(\lambda_0 + \lambda'_2)T_{a2}}}{\lambda_0 + \lambda'_2}
\end{aligned} \tag{4.12}$$

At the end, the error probability given R_1, R_2 both makes correct decisions is defined as

$$\begin{aligned}
u(\lambda_0, \lambda'_0, \lambda_1, \lambda'_1, \lambda_2, \lambda'_2) & = h(\lambda_0, \lambda'_0, T_{a1} + T_{a2})h(\lambda_1, \lambda'_1, -T_{a1})h(\lambda_2, \lambda'_2, -T_{a2}) \\
& \quad + h(\lambda_0, \lambda'_0, T_{a1} - T_{a2})h(\lambda_1, \lambda'_1, -T_{a1})[1 - h(\lambda_2, \lambda'_2, T_{a2})] \\
& \quad + h(\lambda_0, \lambda'_0, -T_{a1} + T_{a2})[1 - h(\lambda_1, \lambda'_1, T_{a1})]h(\lambda_2, \lambda'_2, -T_{a2}) \\
& \quad + h(\lambda_0, \lambda'_0, -(T_{a1} + T_{a2})) [1 - h(\lambda_1, \lambda'_1, T_{a1})][1 - h(\lambda_2, \lambda'_2, T_{a2})] \\
& \quad + m(\lambda_0, \lambda'_0, \lambda_1, \lambda'_1, T_{a2})h(\lambda_2, \lambda'_2, -T_{a2}) \\
& \quad + m(\lambda_0, \lambda'_0, \lambda_1, \lambda'_1, -T_{a2})[1 - h(\lambda_2, \lambda'_2, T_{a2})] \\
& \quad + m(\lambda_0, \lambda'_0, \lambda_2, \lambda'_2, T_{a1})h(\lambda_1, \lambda'_1, -T_{a1}) \\
& \quad + m(\lambda_0, \lambda'_0, \lambda_2, \lambda'_2, -T_{a1})[1 - h(\lambda_1, \lambda'_1, T_{a1})] \\
& \quad + n_1(\lambda_0, \lambda'_0, \lambda_1, \lambda'_1, \lambda_2, \lambda'_2, T_{a1}, T_{a2}) \\
& \quad + n_1(\lambda_0, \lambda'_0, \lambda_1, \lambda'_1, \lambda_2, \lambda'_2, T_{a1}, T_{a2})
\end{aligned} \tag{4.13}$$

And the error probability of the approximated piecewise-linear detector can be

expressed as

$$\begin{aligned}
P_b = & u(\lambda_0, \lambda'_0, \lambda_1, \lambda'_1, \lambda_2, \lambda'_2) \left(1 - \frac{1}{2 + \bar{\gamma}_{0,1}}\right) \left(1 - \frac{1}{2 + \bar{\gamma}_{0,2}}\right) \\
& + u(\lambda_0, \lambda'_0, \lambda'_1, \lambda_1, \lambda_2, \lambda'_2) \left(\frac{1}{2 + \bar{\gamma}_{0,1}}\right) \left(1 - \frac{1}{2 + \bar{\gamma}_{0,2}}\right) \\
& + u(\lambda_0, \lambda'_0, \lambda_1, \lambda'_1, \lambda'_2, \lambda_2) \left(1 - \frac{1}{2 + \bar{\gamma}_{0,1}}\right) \left(\frac{1}{2 + \bar{\gamma}_{0,2}}\right) \\
& + u(\lambda_0, \lambda'_0, \lambda'_1, \lambda_1, \lambda_2, \lambda'_2) \left(\frac{1}{2 + \bar{\gamma}_{0,1}}\right) \left(\frac{1}{2 + \bar{\gamma}_{0,2}}\right)
\end{aligned} \tag{4.14}$$

Simulation results show this closed-form expression provides a tight approximation. We emphasize here that this formula is only suitable for $T_{a1} = T_{a2}$, which means both relays have the same average error probability.

Assuming $\bar{\gamma}_{0,3} = k_1\bar{\gamma}$, $\bar{\gamma}_{0,1} = \bar{\gamma}_{0,2} = k_2\bar{\gamma}$, $\bar{\gamma}_{1,3} = k_3\bar{\gamma}$, $\bar{\gamma}_{2,3} = k_4\bar{\gamma}$ and taking similar steps as in Section 3.2.3, it can be shown that a high SNR approximation for (4.14) is

$$P_b \approx \frac{1}{\bar{\gamma}^2} \frac{2}{k_1 k_2}. \tag{4.15}$$

This high SNR approximation suggest that cooperative diversity with two parallel decoding relays achieves diversity order 2. This coincides with the lower bound of diversity order provided in (3.22) with $M = 3$, and might suggest that the lower bound in (3.22) is tight. It is interesting to note that this high SNR approximation does not rely on the distances between the relays and destination. This is different from (3.15), in which the high SNR approximation relies on the distance between relay and destination. Whether or not this has broader implications is not yet clear.

Simulation results of cooperative diversity with two parallel relays are presented in Figs 4.4–4.6. It is assumed in the simulation that both relays are located at the same position and share the same power with source under the total power constraint, *i.e.*, $E_0 = E_1 = E_2 = 1/3$. The curves of (4.14) overlap with the corresponding curves representing simulation results with nonlinear ML detectors. This shows the tightness of the PL approximation. The curves for the high SNR approximation (4.15) are also presented in the plots. It is easy to see that the high SNR approximation is already tight in moderate SNR regimes for the two cases when relays are not close to the source. However, Fig. 4.4 seems to suggest that this high SNR approximation is not very tight in moderate SNR regimes for the case in

which two relays are both sitting quite close to the source, *i.e.*, [0.1,0]. But, if SNR is increased up to 80 dB, the curve of (4.14) eventually overlaps with the curve of (4.15). The reason is that in high SNR approximation, we throw away high order terms of SNR such as $c/\bar{\gamma}^3$, where c is a constant determined by network geometry. Although such terms are negligible as SNR approaches infinity, these high order terms might still have significant impact at moderate SNR when the relays are close to the source. Among the three scenarios simulated here, cooperative diversity with two relays performs best when the relays are located at [0.1,0]. But in cooperative diversity with one relay, the scenario in which the relay is located at [0.5,0] offers better performance than the scenario in which the relay is located at [0.1,0]. These different observations suggest the optimum location for relays might be close to the source as the number of relays increases. Future work is expected to fully address this problem.

4.3 Noncoherent Cooperative Diversity With Two Receive Antennas

In [27, 26], it has been shown that cooperative diversity can be exploited on top of the spatial diversity provided by multiple antennas. We here provide a closed-form approximation of the uncoded bit error rate for noncoherent cooperative diversity with two receive antennas at the destination. Specifically, the first antenna $RX1$ receives $y_{01}^{(1)}, y_{02}^{(1)}$ from the source and $y_{11}^{(1)}, y_{12}^{(1)}$ from the relay. The second antenna $RX2$ receives $y_{01}^{(2)}, y_{02}^{(2)}$ and $y_{11}^{(2)}, y_{12}^{(2)}$, respectively from the source and the relay.

Assuming the signals received by the two antennas suffer identically independent distributed fading if they came from the same transmitter, the ML detector can be implemented by a detector as shown in Fig. 4.7. The function $g_i(\cdot, \cdot)$ for $i = 0, 1$ is just the same as (3.3) and $f_1(\cdot)$ is the same as (3.4). It is easy to see that Fig. 4.7 is nothing more than a specific example of Fig. 3.2. Therefore, ML detectors for cooperative diversity with multiple receive antennas at the destination can be well incorporated into the general detector structure of normal cooperative diversity.

Applying the PL detector, the approximation for the uncoded bit error rate is

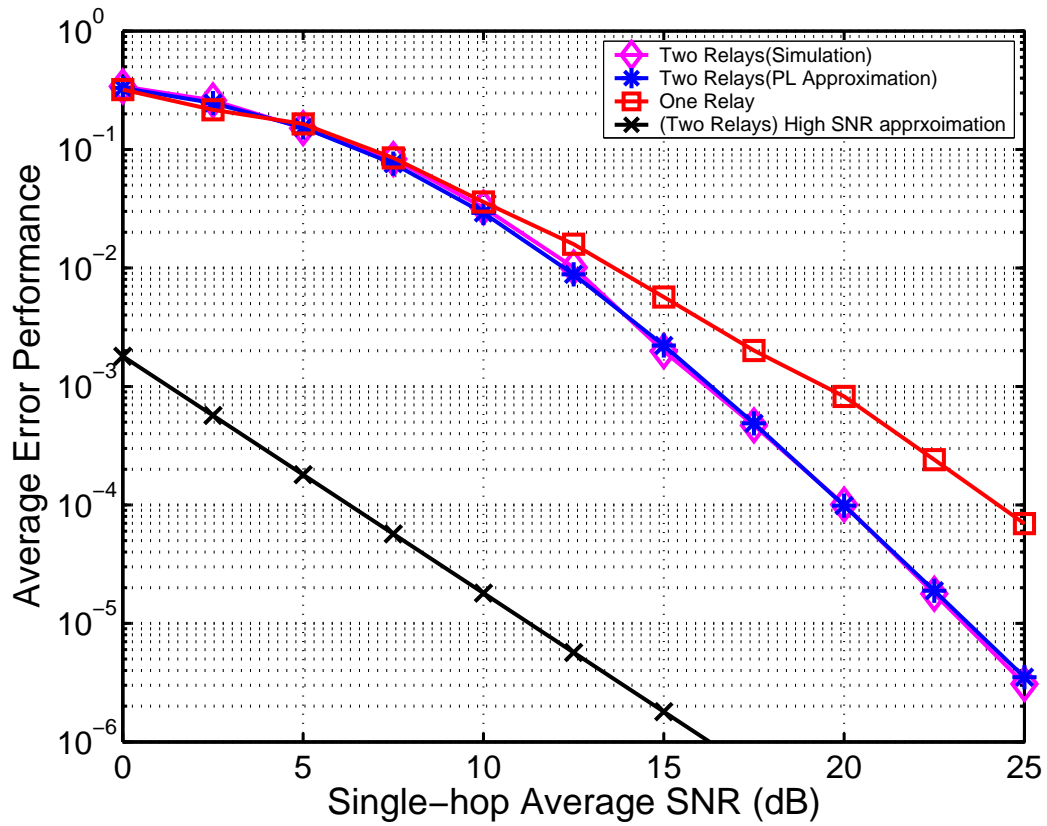


Figure 4.4. Error probability of noncoherent BFSK with two decoding relays. The relays are located at $(0.1, 0)$, *i.e.*, close to the source.

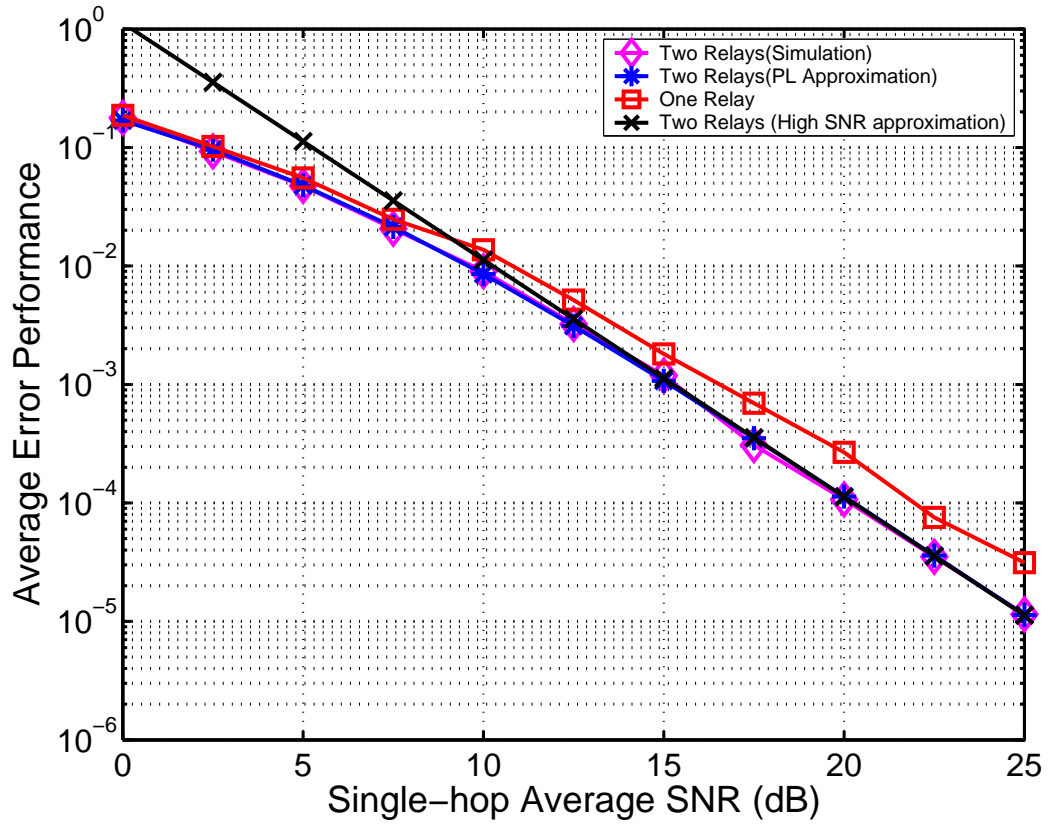


Figure 4.5. Error probability of noncoherent BFSK with two decoding relays. The relays are located at $(0.5, 0)$, *i.e.*, halfway between the source and destination.

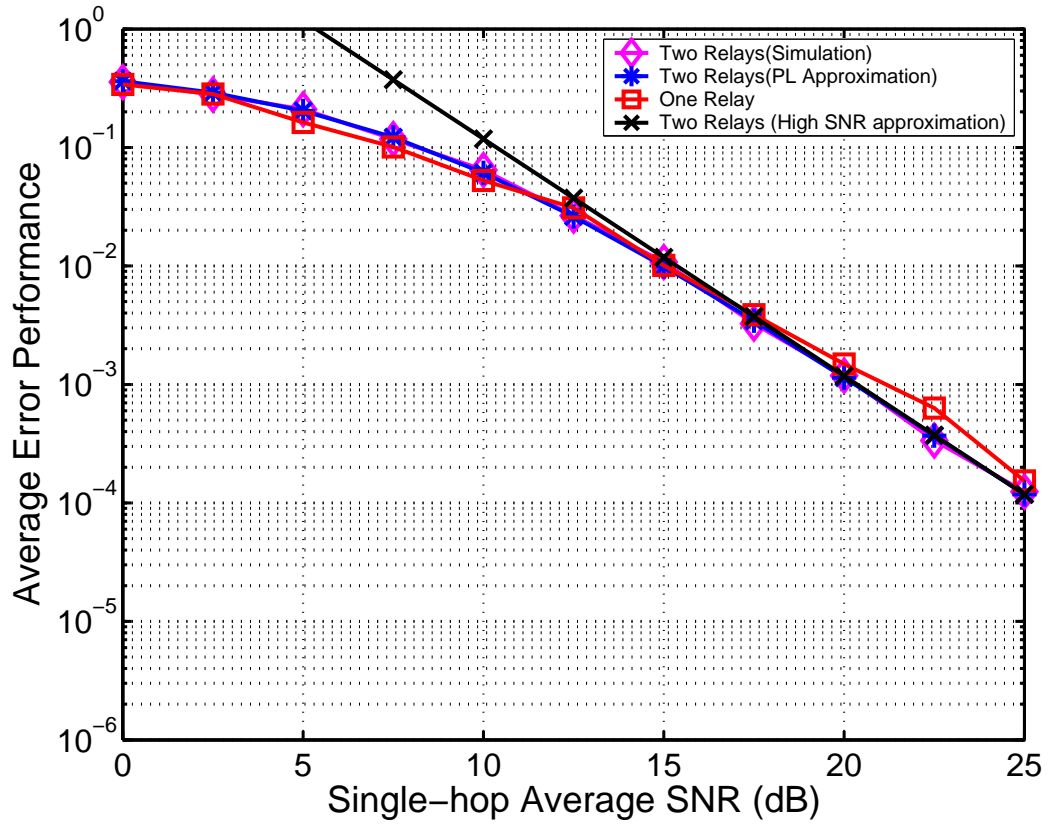


Figure 4.6. Error probability of noncoherent BFSK with two decoding relays. The relays are located at $(0.9,0)$, *i.e.*, close to the destination.

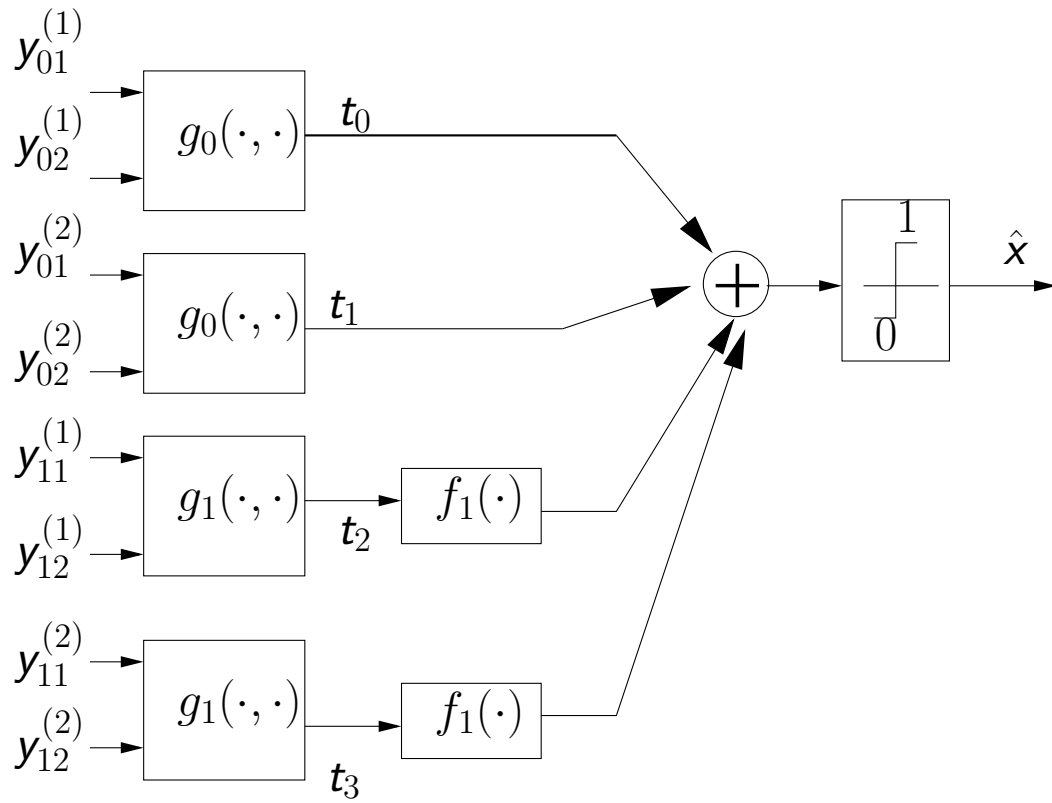


Figure 4.7. Detector for cooperative diversity with two receive antennas.

given as

$$\begin{aligned}
P_b = & G\left(\frac{2}{\bar{\gamma}_{0,2}}, 1 + \frac{2}{\bar{\gamma}_{0,2}}, T_{a1}\right) \times \\
& \left[(1 - \epsilon_1) G\left(\frac{2}{\bar{\gamma}_{1,2}}, 1 + \frac{2}{\bar{\gamma}_{1,2}}, -T_{a1}\right) + \epsilon_1 G\left(1 + \frac{2}{\bar{\gamma}_{1,2}}, \frac{2}{\bar{\gamma}_{1,2}}, -T_{a1}\right) \right] \\
& + G\left(\frac{2}{\bar{\gamma}_{0,2}}, 1 + \frac{2}{\bar{\gamma}_{0,2}}, -T_{a1}\right) \times \\
& \left[1 - (1 - \epsilon_1) G\left(\frac{2}{\bar{\gamma}_{1,2}}, 1 + \frac{2}{\bar{\gamma}_{1,2}}, T_{a1}\right) - \epsilon_1 G\left(1 + \frac{2}{\bar{\gamma}_{1,2}}, \frac{2}{\bar{\gamma}_{1,2}}, T_{a1}\right) \right] \\
& + H_1\left(\frac{2}{\bar{\gamma}_{0,2}}, 1 + \frac{2}{\bar{\gamma}_{0,2}}, \frac{2}{\bar{\gamma}_{1,2}}, 1 + \frac{2}{\bar{\gamma}_{1,2}}, T_{a1}\right) (1 - \epsilon_1) \\
& + H_1\left(\frac{2}{\bar{\gamma}_{0,2}}, 1 + \frac{2}{\bar{\gamma}_{0,2}}, 1 + \frac{2}{\bar{\gamma}_{1,2}}, \frac{2}{\bar{\gamma}_{1,2}}, T_{a1}\right) \epsilon_1 \\
& + H_2\left(\frac{2}{\bar{\gamma}_{0,2}}, 1 + \frac{2}{\bar{\gamma}_{0,2}}, \frac{2}{\bar{\gamma}_{1,2}}, 1 + \frac{2}{\bar{\gamma}_{1,2}}, T_{a1}\right) (1 - \epsilon_1) \\
& + H_2\left(\frac{2}{\bar{\gamma}_{0,2}}, 1 + \frac{2}{\bar{\gamma}_{0,2}}, 1 + \frac{2}{\bar{\gamma}_{1,2}}, \frac{2}{\bar{\gamma}_{1,2}}, T_{a1}\right) \epsilon_1,
\end{aligned} \tag{4.16}$$

where $\bar{\gamma}_{0,2}, \bar{\gamma}_{1,2}$ are the average SNRs per bit, respectively, between the source and destination and between the relay and destination; ϵ_1 is the error probability of the relay; $T_{a1} = \ln\left(\frac{1 - \epsilon_1}{\epsilon_1}\right)$. The functions in (4.16) are defined as following,

$$G(r_1, r_2, x) = \begin{cases} 1 - r_2^2 e^{-r_1 x} (a_1(r_1, r_2)x + a_2(r_1, r_2)) & \text{for } x \geq 0 \\ e^{r_2 x} (a_3(r_1, r_2)x + a_4(r_1, r_2)) & \text{for } x \leq 0 \end{cases} \tag{4.17}$$

where

$$\begin{aligned}
a_1(r_1, r_2) &= \frac{r_1}{(r_1 + r_2)^2}, \\
a_2(r_1, r_2) &= \frac{r_1}{(r_1 + r_2)^2} + \frac{2r_1}{(r_1 + r_2)^3}, \\
a_3(r_1, r_2) &= -r_2 + \frac{r_2^2}{(r_1 + r_2)} + \frac{r_1 r_2^2}{(r_1 + r_2)^2}, \\
a_4(r_1, r_2) &= 1 - \frac{r_2^2}{(r_1 + r_2)^2} - \frac{2r_1 r_2^2}{(r_1 + r_2)^3}, \\
b_1(r_1, r_2) &= \frac{r_1^2}{(r_1 + r_2)^2}, \\
b_2(r_1, r_2) &= \frac{2r_1^2}{(r_1 + r_2)^3}, \\
b_3(r_1, r_2) &= \frac{-r_1}{(r_1 + r_2)} + \frac{r_1 r_2}{(r_1 + r_2)^2}, \\
b_4(r_1, r_2) &= \frac{1}{(r_1 + r_2)} + \frac{r_1 - r_2}{(r_1 + r_2)^2} - \frac{2r_1 r_2}{(r_1 + r_2)^3}, \\
P_0(r_1, x) &= \frac{1}{r_1} e^{r_1 x}, \\
P_1(r_1, x) &= e^{r_1 x} \left(\frac{x}{r_1} - \frac{1}{r_1^2} \right), \\
P_2(r_1, x) &= e^{r_1 x} \left(\frac{x^2}{r_1} - \frac{2x}{r_1^2} + \frac{2}{r_1^3} \right),
\end{aligned} \tag{4.18}$$

and

$$\begin{aligned}
H_1(r_1, r_2, r_3, r_4, x) &= -r_4^2 a_3(r_1, r_2) b_1(r_3, r_4) [P_2(-r_2 - r_3, x) - P_2(-r_2 - r_3, 0)] \\
&\quad + r_4^2 [a_4(r_1, r_2) b_1(r_3, r_4) - a_3(r_1, r_2) b_2(r_3, r_4)] \times \\
&\quad [P_1(-r_2 - r_3, x) - P_1(-r_2 - r_3, 0)] \\
&\quad + r_4^2 a_4(r_1, r_2) b_2(r_3, r_4) [P_0(-r_2 - r_3, x) - P_0(-r_2 - r_3, 0)],
\end{aligned} \tag{4.19}$$

$$\begin{aligned}
H_2(r_1, r_2, r_3, r_4, x) = & G(r_3, r_4, 0) - G(r_3, r_4, -x) \\
& + r_2^2 r_4^2 b_3(r_3, r_4) a_1(r_1, r_2) [P_2(r_1 + r_4, 0) - P_2(r_1 + r_4, -x)] \\
& + r_2^2 r_4^2 [-a_1(r_1, r_2) b_4(r_3, r_4) + a_2(r_1, r_2) b_3(r_3, r_4)] \times \\
& [P_1(r_1 + r_4, 0) - P_1(r_1 + r_4, -x)] \\
& - r_2^2 r_4^2 a_2(r_1, r_2) b_4(r_3, r_4) [P_0(r_1 + r_4, 0) - P_0(r_1 + r_4, -x)].
\end{aligned} \tag{4.20}$$

Assuming $\bar{\gamma}_{0,2} = k_1 \bar{\gamma}$, $\bar{\gamma}_{0,1} = k_2 \bar{\gamma}$, $\bar{\gamma}_{1,2} = k_3 \bar{\gamma}$, it can be shown that $\lim_{\bar{\gamma} \rightarrow \infty} P_b \bar{\gamma}^2 = 0$ and $\lim_{\bar{\gamma} \rightarrow \infty} P_b \bar{\gamma}^3 = \infty$. This suggests that the diversity order for cooperative diversity with two receive antennas is between 2 and 3.

Figs 4.8–4.10 demonstrate the performance of cooperative diversity with two receive antennas at the destination. The simulation condition follows along the same lines as in Chapter 3. The curves for (4.16) and simulation results are overlapped, which shows that the theoretical prediction following piecewise-linear approximation is very accurate. This further illustrates the power of the piecewise-linear approximation in addition to its implementation advantage. The results from cooperative diversity with a single antenna are also presented in the plots. It is easy to see that the combination of cooperative diversity with two receive antennas at the destination will provide diversity gains. We also present the curves for single-hop with three receive antennas in the same plots. When the relay is close to the destination, there is a crossing between the curve for cooperative diversity with two antennas and the curve for single-hop with three antennas. This shows the system still does not achieve full diversity order 3 as compared with single-hop system with three receive antennas. Similar trends can be identified for the scenario when the relay is located halfway between the source and destination. When the relay is close to the source, the curve for cooperative diversity shows a higher slope than that for single-hop in moderate SNR regime. However, as SNR keeps on increasing, there is a change of slope for the curve of cooperative diversity and the diversity order for this scenarios is still less than 3. Observations here combined with those for cooperative diversity with two relays suggest that, for moderate SNR regime, as the

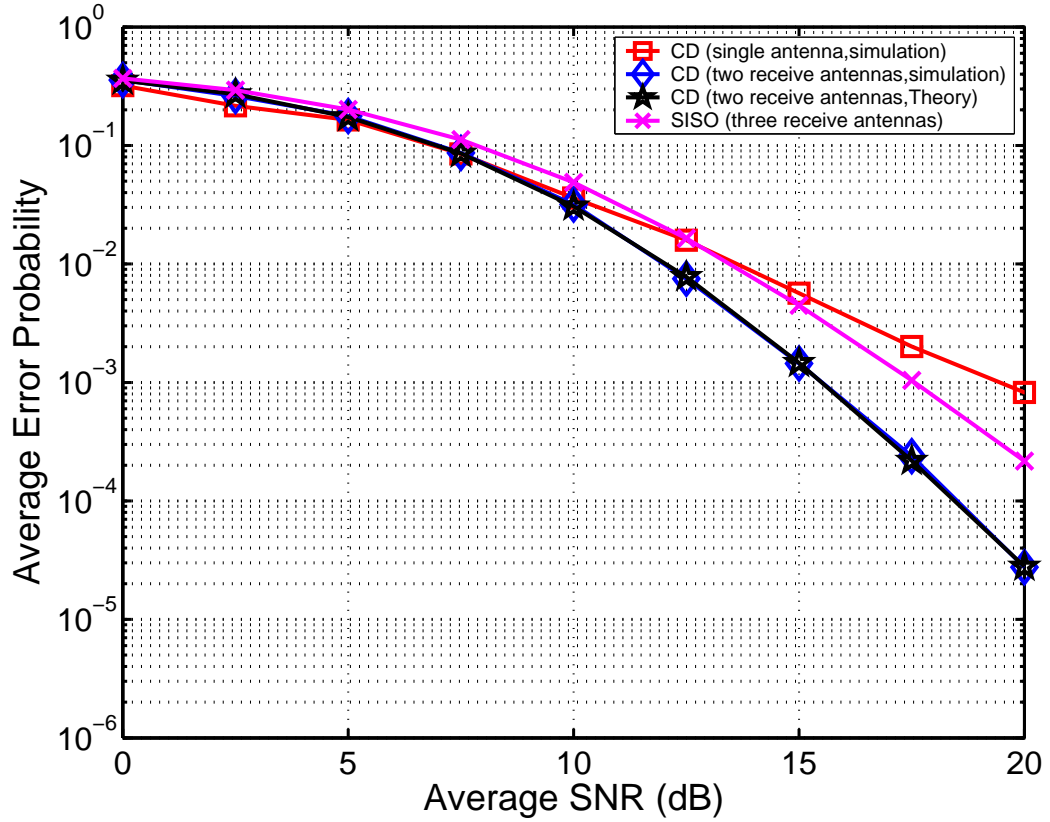


Figure 4.8. Comparison between single-hop with three receive antennas and cooperative diversity with two receive antennas at the destination. The relay is located at $(0.1,0)$, *i.e.*, close to the source.

available diversity order increases, the optimum location for relays to achieve the maximum coding gain is probably close to the source.

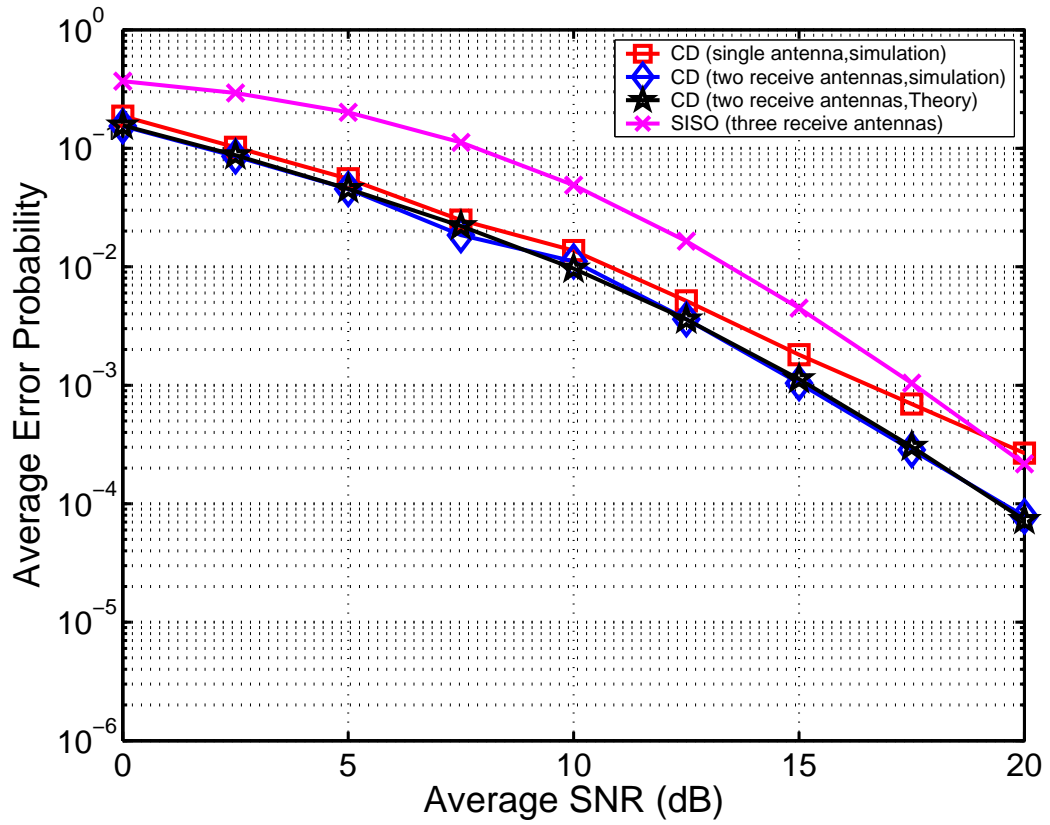


Figure 4.9. Comparison between single-hop with three receive antennas and cooperative diversity with two receive antennas at the destination. The relay is located at $(0.5,0)$, *i.e.*, halfway between the source and destination.

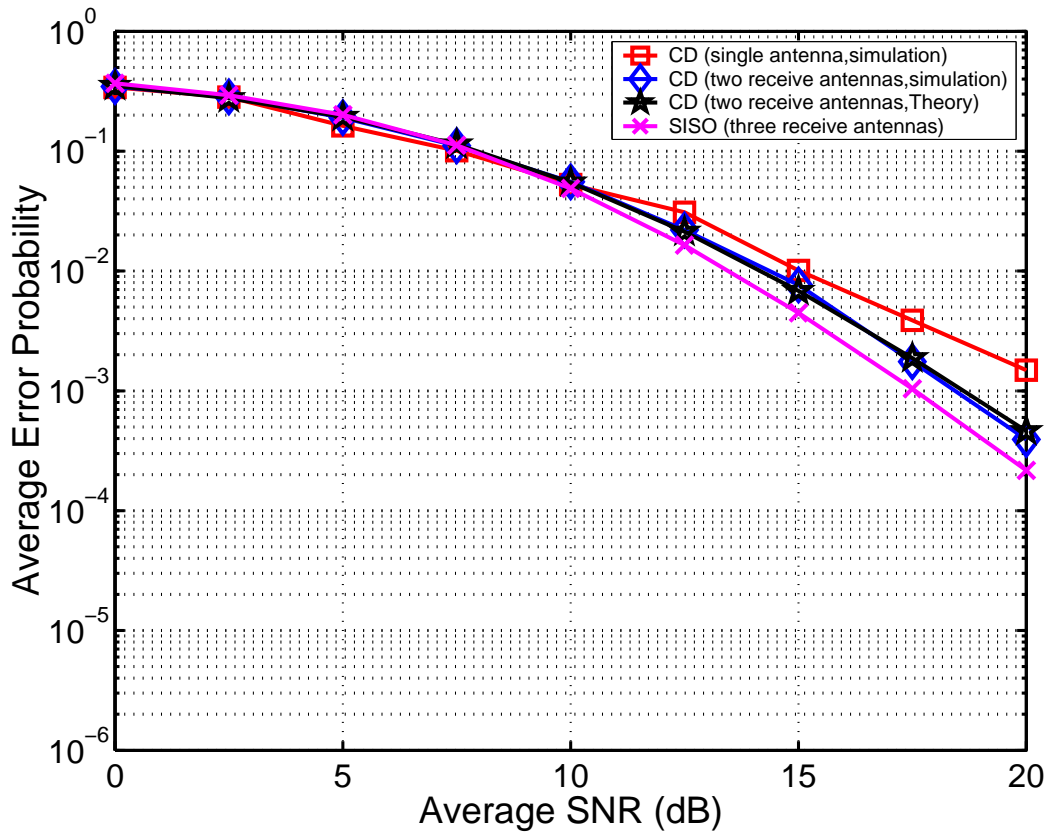


Figure 4.10. Comparison between single-hop system with three receive antennas and cooperative diversity with two receive antennas at the destination. The relay is located at $(0.9,0)$, *i.e.*, close to the destination.

CHAPTER 5

APPLICATION OF CONVOLUTIONAL CODES IN COOPERATIVE DIVERSITY

5.1 Introduction

This chapter focuses on the application of coding techniques to cooperative diversity and provides some results.

We showed in Chapter 3 that noncoherent cooperative diversity substantially improves the performance, in terms of uncoded BER, compared to non-cooperative single-hop transmission. However, the orthogonal channel assumption in cooperative diversity requires the relay not to transmit and receive at the same time. Therefore, the spectral efficiency of cooperative diversity is essentially half that of single-hop. Thus a simple conclusion based on the uncoded BER that cooperative diversity is better than single-hop looks premature. This has motivated us to explore the performance of cooperative diversity with channel coding. With coding, we are able to compare cooperative diversity and single-hop under the constraint of the same spectral efficiency.

Two of the most popular coding schemes are linear block and convolutional codes. The complexity of ML decoding algorithms for linear block codes grows exponentially with the block length. Therefore, in this thesis, we focus on convolutional codes as the Viterbi algorithm provides a convenient way for the decoding of convolutional codes. The complexity of Viterbi algorithm grows exponentially with the constraint length, which is often short. In particular, the analysis is mainly focused on the rate $1/n$ codes as this is the most common code. We again focus on the case of a single relay for simplicity of exposition.

5.1.1 Summary of Assumptions and Results

We consider two types of channels, namely independent identically distributed (i.i.d.) fading channels and block fading channels. They are classified according to the relationship between the coherence time and the symbol time [1]. For an i.i.d fading channel, the coherence time is as short as the symbol duration and the different fading coefficients between symbols are independent. On the other hand, for a block fading channel, a common model [18] assumes that fading coefficients remain constant during one coherence interval and change independently between these intervals. In the following, we refer to the fading coefficients during the same coherence interval as the fading block. Even though the coherence interval might cover more than one symbol period, we can still model the channel as an i.i.d fading channel if the allowable delay constraint is much larger than the coherence time. In this case, an interleaver can be employed and essentially converts the channel into an i.i.d. fading channel [20].

Among the many choices of signal processing schemes for the relay [13, 9, 8], this chapter only focuses on decode-and-forward with symbol-by-symbol demodulation at the relay. This processing differs from the “coded cooperation” proposed in [8]. Coded cooperation requires the relay to decode an entire coded frame from the source to the destination. The relay verifies whether it receives the information correctly using a cyclic redundancy check (CRC). Accordingly, it then decides whether it should send its partner’s information or its own information. A heavily protected overhead has to be inserted into each sequence sent by the relay to denote the owner of the information. Also, coded cooperation requires extra memory at the relay to store the frame in order to make the decision. Symbol-by-symbol demodulation at the relay allows for a low-complexity relay as it does not have any of these issues, and therefore might be easier to be incorporate into wireless networks. Throughout this chapter, all of the discussion is about the decode-and-forward protocol unless otherwise specified. Again, the previous works [13, 9, 8] focus on coherent decoding and we focus mainly on noncoherent decoding.

The remainder of this chapter is organized as follows. Section 5.2 describes the notation and model used in this chapter. Section 5.3 provides noncoherent ML sequence detectors for cooperative diversity with convolutional codes in the i.i.d.

fading channel. The technique of Bhattacharyya upper bound is used to analyze the ML detector's performance. Section 5.3.3 discusses issues of cooperative diversity in the block fading channel. We illustrate the difficulty and complexity of noncoherent ML detection in the block fading channel. Section 5.4 provides the simulation results to support the conclusions drawn from the previous sections.

In summary, we establish:

1. Noncoherent ML sequence detectors for cooperative diversity with convolutional codes in the i.i.d. fading channel. These detectors can be easily implemented by the Viterbi algorithm. Our analysis provides a common expression of Bhattacharyya upper bounds for cooperative diversity in the i.i.d. fading channel with different signaling, namely noncoherent BFSK, coherent BFSK and BPSK. The expression shows that, in high SNR regimes, the free distance of the convolutional code is a key factor for coding performance in cooperative diversity for the i.i.d. fading channel. This common expression also indicates that there is an about 3 dB loss for noncoherent BFSK comparing with coherent BFSK for cooperative diversity in the i.i.d. fading channel.
2. The diversity order for noncoherent cooperative diversity with convolutional codes is less than $2d_{\text{free}}$ in the i.i.d. fading channel. The loss of diversity gain in cooperative diversity may come from the choice of the decode-and-forward protocol at the relay. Given that single-hop and cooperative diversity use maximum free distance convolutional codes with the same constraint length, and rates $1/2n$ and $1/n$, respectively, the analysis indicates that cooperative diversity does not perform better than single-hop in the noncoherent i.i.d. fading channel.

It is also illustrated that noncoherent ML sequence detectors are very complex in the block fading channel. Its complexity prevents further analysis as well as numerical simulation. Therefore, we use noncoherent ML detectors for the i.i.d. fading channel as suboptimal detectors for the block fading channel to simulate the performance of the convolutional codes in the noncoherent block fading channel. Numerical results indicate that cooperative diversity performs better than single-hop in the block fading channel.

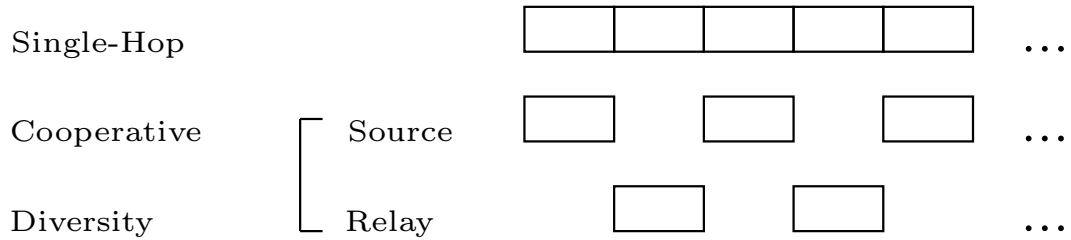


Figure 5.1. Diagram of channel uses by single-hop and cooperative diversity. Each block indicates a symbol transmitted in channel.

5.2 System Model

5.2.1 Notation

We express in the sequel the sequence of binary bits as a vector¹. For example, we use \mathbf{x}_0 to represent a sequence of code bits from the source, and x_{0i} to denote its corresponding i th element. The convolutional code can be expressed as a trellis diagram with many paths representing different code words. We denote the sequence corresponding to the m th path of this trellis as \mathbf{x}_0^m and the i th bit of this sequence as x_{0i}^m .

5.2.2 Model

Focusing on the case of one relay, the source encodes the information bits with a rate $2/n$ code into a sequence \mathbf{x}_0 with length N , and transmits the coded, BFSK modulated signals for this sequence to the relay and destination in the first sub-channel. As shown in Fig. 5.1, an empty symbol period is inserted between each two symbols sent by the source. For every code bit x_{0i} , the relay and destination receive y_{1i}, y_{0i} , respectively. The relay demodulates the signals symbol-by-symbol and transmits its estimate as x_{1i} to the destination utilizing empty symbol periods inside the source sequence. Here, we assume perfect synchronization between the source and relay to avoid collision. Assuming that the destination knows the average error probability of relay, the choice of decode-and-forward enables us to easily express the distribution of the received signals by the destination as well as to utilize some

¹Please refer to Section 3.1.1 for the more detailed explanation of notation for vectors and elements.

results from Chapter 3. Overall, the destination receives signals \mathbf{y}_0 from the source and \mathbf{y}'_1 from the relay. The length of both vectors is N . To make the notation more compact, we also denote \mathbf{y}_0 as \mathbf{y}'_0 .

The comparison between cooperative diversity and single-hop focuses on two different constraints, namely the same spectral efficiency constraint and the same code rate constraint. To have a fair comparison, both cooperative diversity and single-hop have the same number of channel uses, *i.e.*, $2N$, as indicated in Fig. 5.1. To achieve the same spectral efficiency, this thesis makes the code rate of single-hop half that of cooperative diversity. Suppose cooperative diversity must use a rate $1/n$ code, then single-hop uses a rate $1/2n$ code. With a rate $1/n$ code, the number of information bits is N/n for $2N$ channels uses in cooperative diversity. For single-hop, $2N$ channel uses with a rate $1/2n$ code also result in transmission of N/n information bits. Thus, the spectral efficiencies for cooperative diversity with a rate $1/n$ code and single-hop with a rate $1/2n$ are the same. For the same code rate constraint, single-hop uses the same code as cooperative diversity with a rate $1/n$. Thus, single-hop will transmit $2N/n$ information bits and cooperative diversity will transmit N/n information bits for $2N$ channel uses under the same code rate constraint.

5.3 Maximum Likelihood Sequence Detection for Noncoherent Cooperative Diversity

This section focuses on ML sequence detection and its performance for noncoherent cooperative diversity with decode-and-forward in the i.i.d fading channel. At the end, the difficulty and complexity of noncoherent ML sequence detection in the block fading channel is also demonstrated.

5.3.1 Detector For I.I.D. Fading Channel

Because of independent noise at the receive antennas, the channel is discrete memoryless [3] given \mathbf{x}_0 in the i.i.d. fading channel model, and therefore,

$$p(\mathbf{y}'_0, \mathbf{y}'_1 | \mathbf{x}_0) = p(\mathbf{y}'_0 | \mathbf{x}_0) p(\mathbf{y}'_1 | \mathbf{x}_0). \quad (5.1)$$

It turns out that the symbol-by-symbol detection at the relay will enable us to

write down the pdfs as

$$\begin{aligned}
p(\mathbf{y}'_0|\mathbf{x}_0) &= \prod_{i=1}^N \frac{\exp \left[-\frac{|y'_{01i}|^2}{(1-x_{0i})E_0\sigma_{a_{0,2}}^2 + N_0} - \frac{|y'_{02i}|^2}{x_{0i}E_0\sigma_{a_{0,2}}^2 + N_0} \right]}{\pi^2[(1-x_{0i})E_0\sigma_{a_{0,2}}^2 + N_0][x_{0i}E_0\sigma_{a_{0,2}}^2 + N_0]}, \\
p(\mathbf{y}'_1|\mathbf{x}_0) &= \prod_{i=1}^N (1-\epsilon_1) \frac{\exp \left[-\frac{|y'_{11i}|^2}{(1-x_{0i})E_1\sigma_{a_{1,2}}^2 + N_0} - \frac{|y'_{12i}|^2}{x_{0i}E_1\sigma_{a_{1,2}}^2 + N_0} \right]}{\pi^2[(1-x_{0i})E_1\sigma_{a_{1,2}}^2 + N_0][x_{0i}E_1\sigma_{a_{1,2}}^2 + N_0]} \\
&\quad + \epsilon_1 \frac{\exp \left[-\frac{|y'_{11i}|^2}{x_{0i}E_1\sigma_{a_{1,2}}^2 + N_0} - \frac{|y'_{12i}|^2}{(1-x_{0i})E_1\sigma_{a_{1,2}}^2 + N_0} \right]}{\pi^2[(1-x_{0i})E_1\sigma_{a_{1,2}}^2 + N_0][x_{0i}E_1\sigma_{a_{1,2}}^2 + N_0]}. \tag{5.2}
\end{aligned}$$

Note that the subscripts here follow similar rules as in Chapter 3. Specifically, $\sigma_{a_{i,j}}^2$ is the variance of the fading coefficients $a_{i,j}$ between terminal i and j , in which 0 denotes the source, 1 denotes the relay, and 2 denotes the destination. N_0 is the variance of the additive white Gaussian noise, and E_i for $i = 0, 1$ correspond to the average power per bit at the source and relay, respectively. ϵ_1 represents the average error probability of the relay for symbol-by-symbol detection. The code bit x_{0i} is the i th element of the source sequence \mathbf{x}_0 . In y'_{kji} , the subscript k denotes the terminal from which this signal is sent; $j = 1, 2$ denotes which dimension in BFSK signaling this signal corresponds to; and i means the received signal is corresponding to the code bit x_{0i} .

Based on (5.1) and (5.2), the path metric for the candidate transmitted sequence \mathbf{x}_0^m is

$$\begin{aligned}
U^m &= \sum_{i=1}^N -\frac{|y'_{01i}|^2}{(1-x_{0i}^m)E_0\sigma_{a_{0,2}}^2 + N_0} - \frac{|y'_{02i}|^2}{x_{0i}^m E_0\sigma_{a_{0,2}}^2 + N_0} \\
&\quad - \frac{|y'_{11i}|^2}{(1-x_{0i}^m)E_1\sigma_{a_{1,2}}^2 + N_0} - \frac{|y'_{12i}|^2}{x_{0i}^m E_1\sigma_{a_{1,2}}^2 + N_0} \\
&\quad + \ln \left\{ 1 - \epsilon_1 + \epsilon_1 \exp \left[\frac{(2x_{0i}^m - 1)E_1\sigma_{a_{1,2}}^2 (|y'_{11i}|^2 - |y'_{12i}|^2)}{(x_{0i}^m E_1\sigma_{a_{1,2}}^2 + N_0)((1-x_{0i}^m)E_1\sigma_{a_{1,2}}^2 + N_0)} \right] \right\}. \tag{5.3}
\end{aligned}$$

The ML decision rule is to find \mathbf{x}_0^m among all possible code words that maximize U^m .

To illustrate more insight into the decoder for cooperative diversity, it is useful to provide some interpretation for the first two terms in (5.3). It can be seen that

the first two terms can be simplified as

$$\begin{aligned}
U_p^m &= \sum_{i=1}^N -\frac{|y'_{01i}|^2}{(1-x_{0i}^m)\mathbb{E}_0\sigma_{a_{0,2}}^2 + N_0} - \frac{|y'_{02i}|^2}{x_{0i}^m\mathbb{E}_0\sigma_{a_{0,2}}^2 + N_0} \\
&= -\sum_{i=1}^N \left[|y'_{01i}|^2 (x_{0i}^m) + |y'_{02i}|^2 (1-x_{0i}^m) \right].
\end{aligned} \tag{5.4}$$

It turns out that (5.4) is just the optimum decision metric for single-hop with code word length N as shown in [20]. Moreover, the first four terms in (5.3) can be simplified as

$$\begin{aligned}
U_{p'}^m &= \sum_{i=1}^N -\frac{|y'_{01i}|^2}{(1-x_{0i}^m)\mathbb{E}_0\sigma_{a_{0,2}}^2 + N_0} - \frac{|y'_{02i}|^2}{x_{0i}^m\mathbb{E}_0\sigma_{a_{0,2}}^2 + N_0} \\
&\quad - \frac{|y'_{11i}|^2}{(1-x_{0i}^m)\mathbb{E}_1\sigma_{a_{1,2}}^2 + N_0} - \frac{|y'_{12i}|^2}{x_{0i}^m\mathbb{E}_1\sigma_{a_{1,2}}^2 + N_0} \\
&= \sum_{i=1}^N -\frac{1}{1+\bar{\gamma}_{0,2}} \left[|y'_{01i}|^2 (x_{0i}^m) + |y'_{02i}|^2 (1-x_{0i}^m) \right] \\
&\quad - \frac{1}{1+\bar{\gamma}_{1,2}} \left[|y'_{11i}|^2 (x_{0i}^m) + |y'_{12i}|^2 (1-x_{0i}^m) \right].
\end{aligned} \tag{5.5}$$

This can be regarded as the weighted sum of soft-decoding metrics for each sub-channel and is the ML metric for a point-to-point communication scheme with two receive antennas. The last term of (5.3) compensates the uncertainty introduced by the processing of the relay. It is clear that (5.3) can be implemented with the Viterbi algorithm if a convolutional code is employed.

5.3.2 Analysis of Performance

Two error probabilities to evaluate the performance of a convolutional code are the first error event probability and bit error probability. Both can be represented in terms of the pairwise error probability P_d as following [29],

$$\begin{aligned}
P_E &\leq \sum_{d=d_{\text{free}}}^{\infty} a(d)P_d, \\
P_b &\leq \sum_{d=d_{\text{free}}}^{\infty} c(d)P_d,
\end{aligned} \tag{5.6}$$

where $a(d), c(d)$ are the coefficients of

$$\begin{aligned} T(D) &= \sum_{d=d_{\text{free}}}^{\infty} a(d)D^d, \\ \left. \frac{dT(D, N)}{dN} \right|_{N=1} &= \sum_{d=d_{\text{free}}}^{\infty} c(d)D^d, \end{aligned} \quad (5.7)$$

and the $T(D)$ and $T(D, N)$ are the transfer functions obtained from the state diagram. Here $a(d)$ is the number of code words of weight d , and $c(d)$ is the total number of nonzero information bits on all paths with weight d . The length of the transmitted sequence is assumed to be infinite here. If the code is truncated periodically, the summation in (5.6) should go from d_{free} to the finite length of the code word. The pairwise error probability P_d denotes the probability of error at a node where one of the incorrect paths merging with the correct path accumulates higher total metric value. This incorrect path differs in d bits from the correct path. We focus on the criterion of the BER P_b .

As pointed out by [16], in high SNR regimes, the predominant term in (5.6) would be the term with the minimum free distance d_{free} . Therefore, we have a more loose bound for the bit error probability in high SNR regime as follows,

$$P_b \lesssim c(d_{\text{free}})P_{d_{\text{free}}}. \quad (5.8)$$

The above paragraphs present a brief summary about how to evaluate the performance of the convolutional code in terms of pairwise error probability. Interested readers can refer to [16, 29, 20] for more details.

With soft decoding, the pairwise error probability of mistakenly decoding \mathbf{x}_0^m into $\mathbf{x}_0^{m'}$, two codewords that differ in d bits, can be written as

$$P_d = \Pr \left(\sum_{i=1}^d t_{0i} + \ln \frac{(1 - \epsilon_1) \exp t_{1i} + \epsilon_1}{\epsilon_1 \exp t_{1i} + 1 - \epsilon_1} < 0 \right), \quad (5.9)$$

where

$$\begin{aligned} t_{0i} &= \frac{\bar{\gamma}_{0,2}}{N_0(1 + \bar{\gamma}_{0,2})} (|y'_{01i}|^2 - |y'_{02i}|^2), \\ t_{1i} &= \frac{\bar{\gamma}_{1,2}}{N_0(1 + \bar{\gamma}_{1,2})} (|y'_{11i}|^2 - |y'_{12i}|^2). \end{aligned} \quad (5.10)$$

Unlike the single-hop channel, the summation inside (5.9) does not belong to the general quadratic form of complex-valued Gaussian random variables [20]. Nor

is it easy to get the pdf of every term and use the method of moment generating functions [25] to obtain the pdf. A simple upper bound can be provided as,

$$P_d \leq \sum_{i=1}^d \Pr \left(t_{0i} + \ln \frac{(1 - \epsilon_1) \exp t_{1i} + \epsilon_1}{\epsilon_1 \exp t_{1i} + 1 - \epsilon_1} < 0 \right), \quad (5.11)$$

Another lower bound can also be obtained similarly, as follows,

$$P_d \geq \prod_{i=1}^d \Pr \left(t_{0i} + \ln \frac{(1 - \epsilon_1) \exp t_{1i} + \epsilon_1}{\epsilon_1 \exp t_{1i} + 1 - \epsilon_1} < 0 \right). \quad (5.12)$$

The individual term in (5.11) and (5.12) has a closed-form approximation (3.8). However, as we might expect, these bounds are quite loose.

Although it might be possible to employ the piecewise-linear technique on (5.9) to obtain a closed-form expression, the complexity of derivation grows quickly with d , as shown in Section 4.2. The whole deriving process is very cumbersome, and, in view of the involved form of (3.8), the expression for (5.9) can be much more involved to yield any insight.

Instead, we apply the Bhattacharyya upper bound [10] to gain some insight for the governing parameters on the pairwise error probability,

$$\begin{aligned} P_d &\leq \int_{\mathbf{y}} \{p(\mathbf{y}|\mathbf{x}_0^m)p(\mathbf{y}|\mathbf{x}_0^{m'})\}^{1/2} d\mathbf{y} \\ &\leq \int_{\mathbf{y}_0} \{p(\mathbf{y}_0|\mathbf{x}_0^m)p(\mathbf{y}_0|\mathbf{x}_0^{m'})\}^{1/2} d\mathbf{y}_0 \int_{\mathbf{y}'_1} \{p(\mathbf{y}'_1|\mathbf{x}_0^m)p(\mathbf{y}'_1|\mathbf{x}_0^{m'})\}^{1/2} d\mathbf{y}'_1. \end{aligned} \quad (5.13)$$

As mentioned before, the length of the vector is assumed to be N and we have,

$$\int_{\mathbf{y}_0} \{p(\mathbf{y}_0|\mathbf{x}_0^m)p(\mathbf{y}_0|\mathbf{x}_0^{m'})\}^{1/2} d\mathbf{y}_0 = \prod_{i=1}^N \left[\frac{4(1 + \bar{\gamma}_{0,2})}{(2 + \bar{\gamma}_{0,2})^2} \right]^{d_i} = \left[\frac{4(1 + \bar{\gamma}_{0,2})}{(2 + \bar{\gamma}_{0,2})^2} \right]^d, \quad (5.14)$$

and

$$\begin{aligned} \int_{\mathbf{y}'_1} \{p(\mathbf{y}'_1|\mathbf{x}_0^m)p(\mathbf{y}'_1|\mathbf{x}_0^{m'})\}^{1/2} d\mathbf{y}'_1 &= \prod_{i=1}^N \left[2\sqrt{\epsilon_1(1 - \epsilon_1)} + \sqrt{2\epsilon_1^2 - 2\epsilon_1 + 1} \frac{4(1 + \bar{\gamma}_{1,2})}{(2 + \bar{\gamma}_{1,2})^2} \right]^{d_i}, \\ &= \left[2\sqrt{\epsilon_1(1 - \epsilon_1)} + \sqrt{2\epsilon_1^2 - 2\epsilon_1 + 1} \frac{4(1 + \bar{\gamma}_{1,2})}{(2 + \bar{\gamma}_{1,2})^2} \right]^d \end{aligned} \quad (5.15)$$

where d_i is the binary Hamming distance between the i th elements of \mathbf{x}_0^m and $\mathbf{x}_0^{m'}$, d is the total Hamming distance between \mathbf{x}_0^m and $\mathbf{x}_0^{m'}$, and $\epsilon_1 = 1/(2 + \bar{\gamma}_{0,1})$ is the

average bit error rate of the relay. We have utilize the inequality $\sqrt{a+b+c} \leq \sqrt{a} + \sqrt{b} + \sqrt{c}$ in the derivation.

Noticing the expressions (5.14) and (5.15) depend on the total Hamming distance d between the two code words rather than the length of the sequence, a high SNR approximation can be,

$$P_d \lesssim \left(\frac{4}{\bar{\gamma}_{0,2}} \right)^d \left[\sqrt{\frac{4}{\bar{\gamma}_{0,1}}} + \frac{4}{\bar{\gamma}_{1,2}} \right]^d. \quad (5.16)$$

By (5.8), we have the upper bound

$$P_b \lesssim c(d_{f1}) \left(\frac{4}{\bar{\gamma}_{0,2}} \right)^{d_{f1}} \left[\sqrt{\frac{4}{\bar{\gamma}_{0,1}}} + \frac{4}{\bar{\gamma}_{1,2}} \right]^{d_{f1}}, \quad (5.17)$$

for noncoherent cooperative diversity in the i.i.d. fading channel with d_{f1} denotes the free distance of the convolutional code used by cooperative diversity.

This type of upper bound (5.17) removes the dependency of (5.15) and (5.14) on the particular length and distance property of the transmitted sequence. This removal facilitates the comparison of cooperative diversity and single-hop under the same spectral efficiency for they have different number of transmitted symbols for the same time period under this constraint. This upper bound thus enables us to compare cooperative diversity and single-hop as long as the distance properties of the codes for these two different schemes are known.

The upper bound (5.17) demonstrates that the free distance d_{free} for the convolutional code might be the key design parameter for noncoherent i.i.d. fading channel [1]. This fact arises from the i.i.d. assumption in channel.

The upper bound (5.17) for cooperative diversity depends not only on the total Hamming distance between code vectors \mathbf{x}_0^m and $\mathbf{x}_0^{m'}$, but also the network topology among the source, relay and destination. This observation suggests that optimizing the location of relay is still important to the performance of cooperative diversity with coding. Indeed, as we will see later, it might be critical in terms of improving BER in the moderate SNR regime. However, as it can be easily verified by substituting (3.14), this upper bound (5.17) suggests that cooperative diversity with decode-and-forward does not achieve full diversity order, *i.e.*, $2d_{\text{free}}$, where 2 should come from the spatial diversity and d_{free} should come from the time diversity of the

i.i.d. fading channel. This observation combining with results in Section 3.2.4 suggest that the loss of diversity gain may come from the choice of symbol-by-symbol demodulation at the relay.

Moreover, it turns out that we can express this upper bound of BER for i.i.d. fading channel in cooperative diversity as

$$P_b \lesssim c(d_{f1}) \left(\frac{k}{\bar{\gamma}_{0,2}} \right)^{d_{f1}} \left[\sqrt{\frac{k}{\bar{\gamma}_{0,1}}} + \frac{k}{\bar{\gamma}_{1,2}} \right]^{d_{f1}}, \quad (5.18)$$

where different values of k correspond to different modulation schemes, *i.e.*, $k = 2$ corresponds to coherent orthogonal BFSK, $k = 4$ corresponds to noncoherent orthogonal BFSK. It can be easily verified that $k = 1$ is corresponding to coherent BPSK. This interesting observation suggests that noncoherent BFSK in cooperative diversity loses about 3 dB relative to coherent BFSK. As in [20], the error probability for uncoded single-hop system in fading channel can also be represented as $P_b = \frac{k}{4\bar{\gamma}}$, where different k represents different modulation schemes. It happens that in both cases the same modulation schemes are represented by the same k values. It is not clear at the current state whether this interesting observation has broader implications.

To facilitate the comparison between cooperative diversity and single-hop, we provide an upper bound for single-hop with noncoherent BFSK in the i.i.d. fading channel as

$$P_b \lesssim c(d_{f2}) \left(\frac{1}{\bar{\gamma}} \right)^{d_{f2}}, \quad (5.19)$$

where d_{f1} denotes the free distance of the convolutional code used by single-hop.

Given cooperative diversity and single-hop are using the same code, (5.17) and (5.19) indicates that cooperative diversity has higher diversity gain and is expected to perform better for asymptotically high SNR.

Under the same spectral efficiency, single-hop uses a rate $1/2n$ code and cooperative diversity uses a rate $1/n$ code. Because both (5.17) and (5.19) suggest maximum free distance codes should be used to achieve lower BERs, we compare cooperative diversity and single-hop assuming maximum free distance codes are used in both schemes. Suppose both codes are maximum free distance codes with the same constraint length, we assume

$$d_{f1} \approx \frac{1}{2}d_{f2}. \quad (5.20)$$

This assumption is justified in the following way. By [20], an upper bound on the free distance of a rate $1/n$ convolutional code is given by

$$d_{\text{free}} \leq \min_{l \geq 1} \left\lfloor \frac{2^{l-1}}{2^l - 1} (K + l - 1)n \right\rfloor \quad (5.21)$$

where $\lfloor x \rfloor$ denotes the largest integer smaller than x , K is the constraint length and l is a variable. Given the same constraint length, (5.21) suggests that maximum free distance of the convolutional code grows linearly with n , which justifies the assumption (5.20). We note that this upper bound is tight for low rate codes. For high rate codes, the free distance is better approximated by the tight lower bound provided in [2]. This lower bound shows a nonlinear relationship between the free distance and code rate.

With the assumption of (5.20) and the same spectral efficiency constraint, (5.17) and (5.19) suggest that cooperative diversity would not significantly outperform single-hop for asymptotically high SNR. This is because the key advantage of cooperative diversity is the spatial diversity provided by the relay being located away from the source. But the i.i.d. fading channel assumption eventually introduces time diversity for every code bit in both single-hop and cooperative diversity. Thus the spatial diversity does not provide extra gains. However, cooperative diversity should still perform better due to the spatial diversity gain if the i.i.d channel assumption is not valid and time diversity gain is very limited. This motivates us to investigate the performance of cooperative diversity in the block fading channel, which provides limited time diversity since the fading coefficients remain constant during a block.

5.3.3 Issues in Noncoherent ML Detection for Block Fading Channel

If the fading channels vary slowly and there is a delay constraint such that full interleaving of codes is impossible, the i.i.d. channel model is no longer valid. In order to better model the correlated fading process, another common fading channel is the block fading channel [18] in which the fading coefficients remain constant during one coherence interval and change independently between these intervals. In

this section, we will see how this change of channel model affects the detection and performance of cooperative diversity.

The impact of this change of the model is immediately reflected in the signaling design of the system. Since the fading coefficients remain unchanged among multiple symbols, differential-phase-shift-keying (DPSK) is a natural choice as it only relies on the phase difference of two adjacent symbols [20] and provides more bandwidth efficiency than BFSK. However, this is under the assumption that we know the exact coherence time since DPSK needs to use the first symbol as a reference [28]. Research for noncoherent communication in the block fading channel is intensively going on [7, 31, 19, 28].

To illustrate the difficulty facing maximum likelihood detection in the block fading channel, we use binary DPSK for it provides more compact notation. As the fading coefficients are independent among different fading blocks, we focus on obtaining the joint pdf of the input signals inside one fading block with length T , given transmitted signals \mathbf{x}_0 and the instantaneous error probability of the relay ϵ_1 ,

$$\begin{aligned} p(\mathbf{y}_0, \mathbf{y}'_1 | \mathbf{x}_0, \epsilon_1) &= p(\mathbf{y}_0 | \mathbf{x}_0, \epsilon_1) p(\mathbf{y}'_1 | \mathbf{x}_0, \epsilon_1) \\ &= \int_{\mathbf{a}_{0,2}} \prod_{i=1}^T p(y_{0i} | \mathbf{x}_{0i}, \epsilon_1) d\mathbf{a}_{0,2} \int_{\mathbf{a}_{1,2}} \prod_{i=1}^T p(y'_{1i} | \mathbf{x}_{0i}, \epsilon_1) d\mathbf{a}_{1,2} \end{aligned} \quad (5.22)$$

The first term can be expressed as,

$$\begin{aligned} \int_{\mathbf{a}_{0,2}} \prod_{i=1}^T p(y_{0i} | \mathbf{x}_i, \epsilon_1) d\mathbf{a}_{0,2} &= \frac{1}{(\pi N_0)^T} \frac{1}{\pi [N_0 + TE_0 \sigma_{\mathbf{a}_{0,2}}^2]} \exp \left\{ -\frac{\left| \sum_{i=1}^T y_i \mathbf{x}_{0i} \right|^2}{[N_0 + TE_0 \sigma_{\mathbf{a}_{0,2}}^2] T} \right\} \\ &\quad \times \exp \left\{ \frac{1}{N_0} \left[-\frac{1}{T} \left| \sum_{i=1}^T y_i \mathbf{x}_{0i} \right|^2 + \sum_{i=1}^T |y_i|^2 \right] \right\}, \end{aligned} \quad (5.23)$$

It turns out that the symbol-by-symbol detection at the relay will enable us to write down the pdf of the second term as,

$$\begin{aligned} \int_{\mathbf{a}_{1,2}} \prod_{i=1}^T p(y'_{1i} | \mathbf{x}_0, \epsilon_1) d\mathbf{a}_{1,2} &= \int_{\mathbf{a}_{1,2}} \frac{1}{(\pi N_0)^T} \prod_{i=1}^T (1 - \epsilon_1) \exp \left[-\frac{1}{N_0} \left| y'_{1i} - (1 - \epsilon_1) \sqrt{E_1} \mathbf{a}_{1,2} \right|^2 \right] \\ &\quad + \epsilon_1 \exp \left[-\frac{1}{N_0} \left| y'_{1i} - \epsilon_1 \sqrt{E_1} \mathbf{a}_{1,2} \right|^2 \right] d\mathbf{a}_{1,2} \end{aligned} \quad (5.24)$$

The difficulty in solving this integral limits our further analysis. Note that (5.24) should be further averaged with respect to the instantaneous error probability of the relay, ϵ_1 , if the destination is assumed to only know the average error probability of the relay. This further complicates the effort of obtaining a ML detector for cooperative diversity in the noncoherent block fading channel. Although efforts are focused on binary DPSK, similar conclusions and observations can also be drawn for BFSK signaling schemes. As the block fading channel poses a particular challenge, we, in the sequel, relies on numerical simulation to gain some hints.

5.4 Numerical Results

The conditions of the simulations presented here largely follow the same lines as in Chapter 3. The convolutional codes used in simulations are the maximum free distance codes chosen from [20]. The constraint length is chosen as 4. For the rate 1/2 code, its generators in octal are 15, 17 and the maximum free distance is 6. For the rate 1/4 code, its generators in octal are 13, 15, 15, 17, and the maximum free distance is 13. We would like to emphasize that we do not provide simulation results for noncoherent ML detection for the block fading channel due to the difficulty illustrated in Section 5.3.3. Instead, we provide simulation results of noncoherent ML detectors for the i.i.d. fading channel working in the block fading channel. This gives us a hint about how the performance in the block fading channel degrades when detectors are designed according to the i.i.d. fading channel.

Fig. 5.2 demonstrates the performance of noncoherent cooperative diversity and single-hop in the i.i.d. fading channel. The crossing of the curves for single-hop with a rate 1/4 code and for cooperative diversity with a rate 1/2 code shows that given the same spectral efficiency, cooperative diversity does not provide much benefit. However, in low SNR regime, cooperative diversity with the relay located at [0.5,0] can have better performance due to the repetition coding gain. Figs 5.3–5.4 provide the performance of ML detectors for the i.i.d. fading channel working in the block fading channel with different lengths of fading blocks. By comparing Figs 5.2–5.4, it can be observed that there is significant degradation of performance in the block fading channel. As time diversity gain is more difficult to exploit in the block fading channel, cooperative diversity with appropriate locations of the relay demonstrates

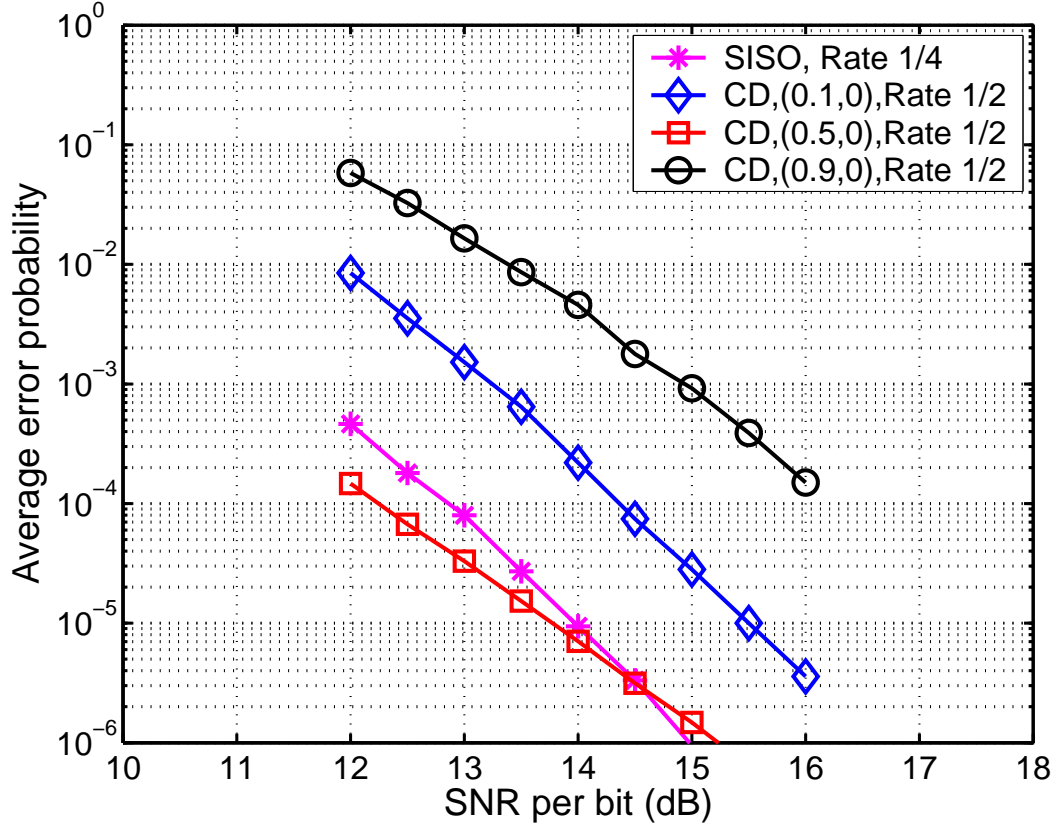


Figure 5.2. Average bit error probability of noncoherent BFSK with the decoding relay located at different locations. Soft decoding based on the Viterbi algorithm is used. The fading coefficients are assumed to be i.i.d. between symbols.

its advantage of spatial diversity gain. In particular, Fig. 5.4 clearly demonstrates that cooperative diversity has higher diversity gain when the block length is long. More promising, even when the length of the fading block is of moderate value, the performance of cooperative diversity shows signs of improvement. This is demonstrated by Fig. 5.3. In Fig. 5.3, the fading block only covers 8 symbol-periods, but the curves for cooperative diversity in block fading channels are below the the curves of the single-hop when the relay is located in $[0.5, 0]$. The gains are roughly 2 dB when the lengths of the fading blocks are 4 and 8 symbol periods. This shows the importance of optimizing the location of the relay.

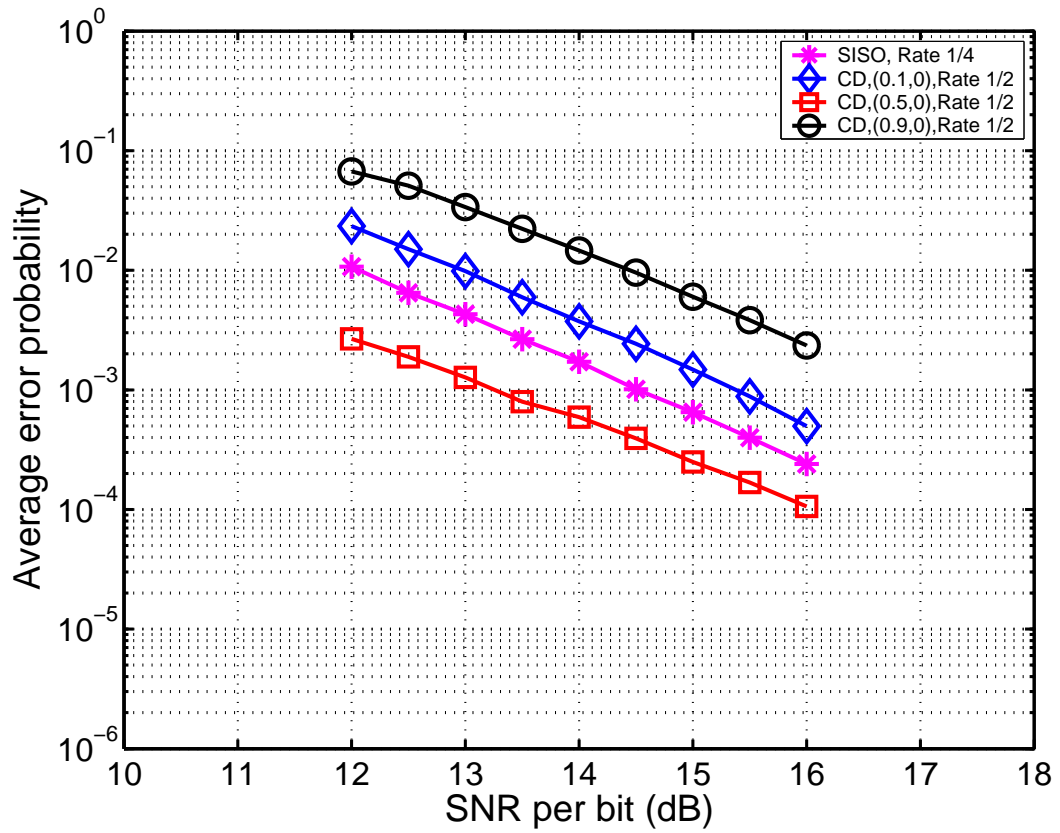


Figure 5.3. Average bit error probability of noncoherent BFSK with the decoding relay located at different locations. Soft decoding based on the Viterbi algorithm is used. The length of the fading block is assumed to cover eight symbol-periods.

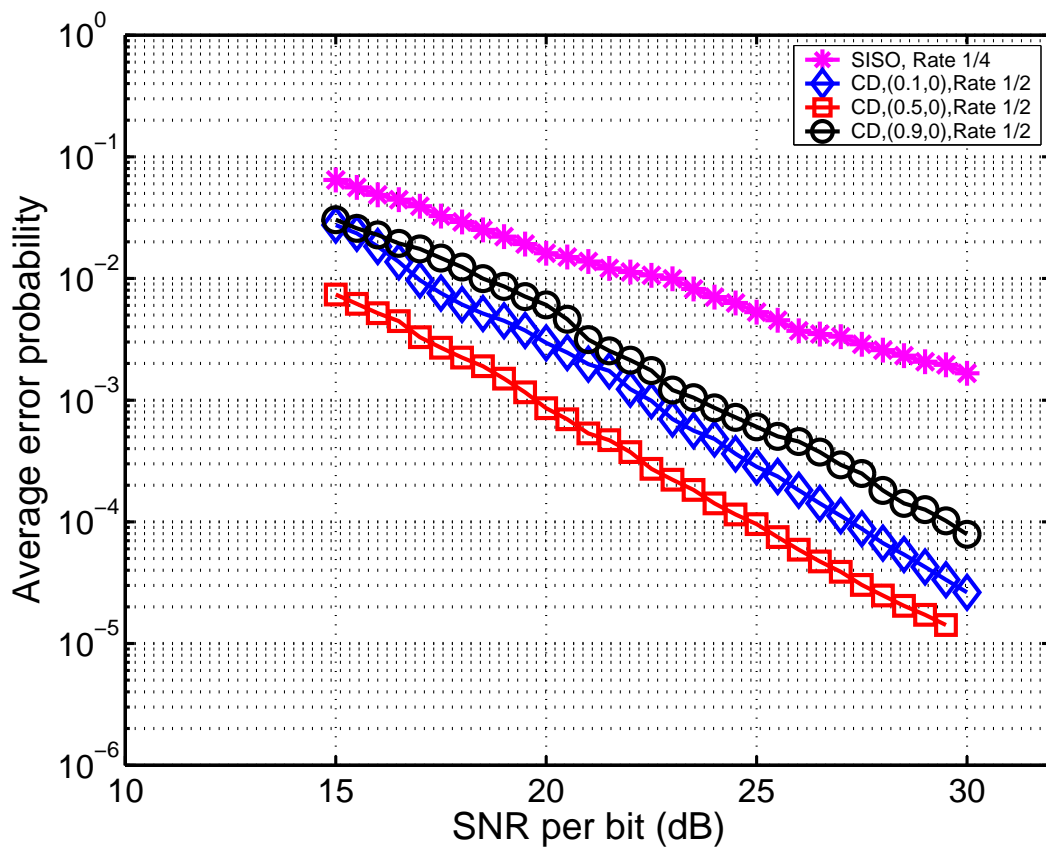


Figure 5.4. Average bit error probability of noncoherent BFSK with the decoding relay located at different locations. Soft decoding based on the Viterbi algorithm is used. The length of the fading block is assumed to cover 128 symbol-periods.

CHAPTER 6

CONCLUDING REMARKS AND FUTURE WORK

The goal of this research has been to explore several of the many issues involved with cooperative diversity for use in fading environments. Specifically, this thesis has addressed several questions related to noncoherent demodulation in these systems, and the results are demonstrated through analysis and simulation.

Chapter 3 proposes a general framework for uncoded maximum likelihood (ML) demodulation in multi-hop and cooperative wireless communication. This chapter focuses on the decode-and-forward protocol for its lack of treatment in the literature as well as its importance in practical systems. In general, ML detectors for cooperative diversity are nonlinear functions. Thus, a piecewise-linear demodulator is developed as an accurate approximation of the ML detector for cooperative diversity. This piecewise-linear detector is easier to implement than the nonlinear ML detector. It also leads to a tight closed-form upper bound for the error probability of the ML detector. A high SNR approximation based on this closed-form expression is presented. This chapter also shows that contrary to coherent case, amplify-and-forward protocol poses a particular challenging problem in the context of noncoherent demodulation.

Chapter 4 extends the techniques of PL approximation to three other cases to show the powers and limitations of PL techniques. It shows that the PL approximation is not limited to noncoherent cooperative diversity with a decoding relay. The PL approximation is applicable to coherent cooperative diversity as well and leads to an integral expression of BER. It provides closed-form BER expressions for noncoherent cooperative diversity with two decoding relays and noncoherent cooperative diversity with two receive antennas at the destination. The complexity of

derivation greatly increases as the number of relay increases and limits our capability of obtaining closed-form BER expressions for cooperative diversity with more than two relays.

Chapter 5 describes the application of coding techniques in cooperative diversity systems. It demonstrates that with symbol-by-symbol detection at the relay, maximum likelihood sequence detection for convolutional codes in the i.i.d. fading channel can be easily realized with a suitably modified Viterbi Algorithm. Using the Bhattacharyya upper bound, the analysis shows that minimum free distance of code words play a key role in determining the performance of coding for cooperative diversity in fading environments. This holds true for both noncoherent and coherent system with i.i.d. fading channel. Given the same spectral efficiency, the simulation results suggest that cooperative diversity can perform better comparing with single-hop in the block fading channel. The reason is that the block fading channel has limited time diversity and cooperative diversity essentially exploits spatial diversity.

Several other important issues have been left for future work. Many of the results of this thesis could be extended formally to multiple relays with the increasing complexity. But a more general technique to get a high SNR approximation is needed for the case of multiple relays. Also, the ML detectors for the amplify-and-forward protocol in noncoherent cooperative diversity is still unresolved. Moreover, in Chapter 5, we limited ourself to symbol-by-symbol detection at relay. More flexible signal processing methods other than decode-and-forward and amplify-and-forward are possible as shown in the literature [8, 9, 35, 17]. A comprehensive review and comparison of different signal processing methods is a key to fully exploiting the benefits offered by cooperative diversity. So far, all research about cooperative diversity has been assuming perfect synchronization of the source and relay. It has not been very clear that how this can be achieved. Resolving this synchronization issue is critical in realization of cooperation diversity. Finally, a demonstration of these schemes within a wireless testbed would provide a useful tool for verifying our analytical results and assumptions.

BIBLIOGRAPHY

- [1] Ezio Biglieri, John Proakis, and Shlomo Shamai(Shitz). Fading channels: Information-theoretic and communication aspects. *IEEE Transaction On Information Theory*, 44(6), 1998.
- [2] Daniel J. Costello. Free distance bounds for convolutional codes. *IEEE Transaction On Information Theory*, 20(3):356–365, May 1974.
- [3] Robert G. Gallager. *Information Theory and Reliable Communication*. John Wiley & Sons, Inc, 1968.
- [4] Hesham El Gamal and Defne Aktas. Distributed space-time filtering for cooperative wireless networks. In *GlobeCom*, 2003.
- [5] Mazen O. Hasna and Mohamed-Slim Alouini. A performance study of dual-hop transmissions with fixed gain relays. In *IEEE International Conference on Acoustics, Speech, and Signal Processing (ICASSP)*, volume 4, pages IV–189–92, 2003.
- [6] Mazen O. Hasna and Mohamed-Slim Alouini. A performance study of dual-hop transmissions with fixed gain relays. *to appear on IEEE Trans. on Wireless Communicatioons*, January 2003.
- [7] Bertrand M. Hochwald and Thomas L. Marzetta. Unitary space-time modulation for multiple-antenna communcations in Rayleigh flat fading. *IEEE Transaction On Information Theory*, 46(2), 2000.
- [8] Todd E. Hunter and Aria Nosratinia. Diversity through coded cooperation. *IEEE Transaction On Wireless Communications*. submitted for publication.
- [9] Mohammand Janani, Ahmadreza Hedayat, Todd E. Hunter, and Aria Norsatinia. Coded cooperation in wireless communications: Space-time transmission and iterative decoding. *IEEE Transaction On Signal Processing*, to appear.
- [10] Gideon Kaplan, Shlomo Shamai (Shitz), and Yosel Kofman. On the design and selection of convolutional codes for and uninterleaved, bursty Rician channel. *IEEE Transaction On Communications*, 43(12), 1995.
- [11] Catherine M. Keller and Michael B. Pursley. Clipped diversity combining for channels with parital-band interference—Part I: Clipped-linear combining. *IEEE Transactions on Communications*, 35(12), 1987.

- [12] J Nicholas Laneman. *Cooperative Diversity in Wireless Networks: Algorithms and Architectures*. PhD thesis, Massachusetts Institute of Technology, August 2002.
- [13] J Nicholas Laneman, David N. C. Tse, and Gregory W. Wornell. Cooperative diversity in wireless networks: Efficient protocols and outage behavior. *IEEE Trans. Inform. Theory*, April 2003. Accepted for publication.
- [14] J Nicholas Laneman and Gregory W. Wornell. Energy-efficient antenna-sharing and relaying for wireless networks. In *Proc. IEEE Wireless Communications and Networking Conference (WCNC)*, 2000.
- [15] J. Nicholas Laneman and Gregory W. Wornell. Distributed space-time coded protocols for exploiting cooperative diversity in wireless networks. *IEEE Transaction On Information Theory*, 59(10), 2003.
- [16] Shu Lin and Daniel J. Costello. *Error Control Coding: Fundamentals and Applications*. McGraw-Hill, Inc, 1983.
- [17] Ruoheng Liu, Predrag Spasojevic, and Emina Soljanin. User cooperation with punctured turbo codes. available at <http://wireless.poly.edu/act/files/dpcccv4.pdf>.
- [18] Robert J. McEliece and Wayne E. Stark. Channels with block interference. *IEEE Transaction On Information Theory*, 30(1), 1984.
- [19] Panayiotis D. Papadimitriou and Costas N. Georghiades. On binary code design for the non-coherent block fading channel. In *GlobeCom*, pages 1603–1607, 2003.
- [20] John G. Proakis. *Digital Communications*. McGraw-Hill, Inc., 1995.
- [21] Theodore S. Rappaport. *Wireless Communications: Principles and Practice*. Prentice-Hall, Inc., 1996.
- [22] Alejandro Ribeiro, Xiaodong Cai, and Georgios B. Giannakis. Symbol error probabilities for general cooperative links. *IEEE Transaction On Wireless Communications*. To Appear, 2004.
- [23] Andrew Sendonaris, Elza Erkip, and Behnaam Aazhang. User cooperation diversity, Part I: System description. *IEEE Transaction On Communications*, 51(11):1927–1938, 2003.
- [24] Andrew Sendonaris, Elza Erkip, and Behnaam Aazhang. User cooperation diversity, Part II: Implementation aspects and performance analysis. *IEEE Transaction On Communications*, 51(11):1939–1948, 2003.
- [25] Marvin K. Simon and Mohamed-Slim Alouini. *Digital Communication over Fading Channels: A Unified Approach to Performance Analysis*. John Wiley & Sons, Inc, 2000.
- [26] Andrej Stefanov and Elza Erkip. Cooperative space-time coding for wireless networks. In *Proceedings of IEEE Information Theory Workshop*, 2003.

- [27] Andrej Stefanov and Elza Erkip. On the performance analysis of cooperative space-time coded system. In *IEEE Wireless Communications and Networking Conference (WCNC)*, 2003.
- [28] Wim Sweldens. Fast block noncoherent decoding. *IEEE Communication Letters*, 5(4), 2001.
- [29] Andrew J. Viterbi and Jim K. Omura. *Principles of Digital Communication and Coding*. McGraw-Hill, Inc, 1979.
- [30] Zhengdao Wang and Georgios B. Giannakis. A simple and general parameterization quantifying performance in fading channels. *IEEE Transaction On Communications*, 51(8):1389–1398, 2003.
- [31] Dilip Warrier and Upamanyu Madhow. Spectrally efficient noncoherent communication. *IEEE Transaction On Information Theory*, 48(3), 2002.
- [32] Frans M.J. Willems. The discrete memoryless multiple access channel with partially cooperating encoders. *IEEE Transaction On Information Theory*, 29(3):441–445, May 1983.
- [33] Frans M.J. Willems and Edward C. van der Meulen. The discrete memoryless multiple access channel with cribbing encoders. *IEEE Transaction On Information Theory*, 31(3):313–327, May 1985.
- [34] Melda Yuksel and Elza Erkip. Diversity in relaying protocols with amplify and forward. In *GlobeCom*, 2003.
- [35] Bin Zhao and Matthew C. Valenti. Distributed turbo coded diversity for the relay channel. *IEE Electronics Letters*, 39(10):786–787, May 2003.